

FMH606 Master's Thesis 2019  
Energy and Environmental Technology

# **Dispersion of hydrogen in confined spaces**

Osama Kabbashi M. Ibrahim

Faculty of Technology, Natural sciences and Maritime Sciences  
Campus Porsgrunn

**Course:** FMH606 Master's Thesis, 2019

**Title:** Dispersion of hydrogen in confined spaces

**Number of pages:** 77

**Keywords:** Tunnel fires, concentration gradients, momentum-controlled jets, buoyancy-controlled jets, hydrogen-air mixture cloud, flame propagation, pressure wave.

<b>Student:</b>	Osama Kabbashi M.Ibrahim
<b>Supervisor:</b>	Prof. Dag Bjerketvedt
<b>External partner:</b>	MoZEES and HyTunnel and CS
<b>Availability:</b>	Open

**Summary:**

Usage of hydrogen as fuel gives rise to possible accidental risks due to leakage and dispersion. The highest risk from hydrogen leak is the formation of a large volume of the hydrogen-air mixture, which could be ignited leading up to a severe explosion. Prevention and control of formation and ignition of hydrogen combustible cloud necessitate sufficient knowledge of mechanisms of the hydrogen leak, dispersion, and over-pressures generated during ignition and explosion.

This study aims to investigate the momentum-controlled jet, the buoyancy-controlled wave and the parameters influence hydrogen concentration distribution in confined spaces. It demonstrates experimental results and analysis from helium and hydrogen dispersion and explosion in a channel. Two groups of experiments were carried out. Firstly, a set of experiments for the release of helium and hydrogen jets in a 3 m long channel to record their concentrations in the cloud by concentration sensors at different horizontal and vertical positions. Secondly, a series of hydrogen explosions in the channel to examine the overpressures built-up during the combustion process and the flame propagation characteristics. Two flow visualization techniques were applied by means of Background-oriented Schlieren and Shadowgraph along with high-speed video camera to image the mixing process around the release point, the helium-, hydrogen-air cloud shape at the middle of the channel and flame evolution after ignition of hydrogen-air mixture cloud. Moreover, results were used for comparison of helium and hydrogen concentration gradients.

Experiments results show swift mixing occurs at higher flow rates, smaller nozzle sizes, and downward release direction. Higher concentration recorded in the channel with negative inclination. Results also confirmed that hydrogen/ helium behavior pattern in the channel accords with mutual intrusion theory about gravity currents. On the question of an explosion of the hydrogen-air mixture in a channel, this study found that for short release time of hydrogen, the highest overpressure was generated when the flame passed through the mixing zone around the jet. For a long time release, the highest overpressure generated after the ignition in the proximity of ignition source. This could be a realistic scenario when hydrogen accumulates after accidental leakage in a tunnel or channel and subsequent ignition of the hydrogen-air cloud.

# Preface

This thesis has been written on the topic “ Dispersion of hydrogen in confined spaces” to accomplish the master program in Energy and Environmental Technology at the University of South-East Norway (USN). This study is a part of a program in the Norwegian center for (FME), mobility zero-emission energy systems (MoZEES) in Research Area 3 (RA3) which focuses on heavy-duty systems, battery, and hydrogen safety issues (project number 257653). In addition, it is also part of the EU Horizon 2020, HyTunnel and CS project concerning the traffic in confined infrastructures in accord with the implementation of EU directive 2004/54/EC and innovative safety measures in case of an accident from hydrogen leak in tunnels. The study has been performed at the laboratory in Faculty of Technology, Natural Sciences, and Maritime Sciences, Campus Porsgrunn.

I would like to express my deep gratitude to Professor Dag Bjerketvedt, my research supervisor, for his patient guidance, valuable and constructive suggestions, and professional assistance during the experimental work. His willingness to give his time so generously has been very much appreciated. I would also like to express my very great appreciation to Professor Knut Vågsæther for his useful recommendations and valuable help.

My grateful thanks are also to extend to my teachers Associated Professors Andre Vagner Gaathaug and Joachim Lundberg for their help during this study. I am particularly grateful for the advice and assistance were given by Associated Professor Per Morten Hansen. Finally, I wish to thank all my friends and my brother for their support and encouragement through my study.

Porsgrunn, May 2019

Osama Kabbashi M.Ibrahim



# Contents

Preface .....	4
Contents.....	5
Nomenclature .....	6
<b>1 Introduction .....</b>	<b>7</b>
1.1 Background .....	7
1.2 Objective.....	7
1.3 Report structure.....	8
<b>2 Hydrogen dispersion .....</b>	<b>9</b>
2.1 Overview of hydrogen dispersion.....	9
2.1.1 <i>Helium: similarity to hydrogen</i> .....	10
2.1.2 <i>Momentum- and buoyancy-controlled jets</i> .....	10
2.1.3 <i>Gravity Currents</i> .....	10
2.1.4 <i>Froude scaling</i> .....	11
2.2 Experimental setup.....	13
2.2.1 <i>Channel description</i> .....	13
2.2.2 <i>Helium injection</i> .....	13
2.2.3 <i>Measurement devices</i> .....	14
2.2.4 <i>Flow visualization techniques</i> .....	15
2.2.5 <i>Experimental models</i> .....	16
2.3 Results and discussion.....	18
2.3.1 <i>Flow rate effects</i> .....	18
2.3.2 <i>Nozzle size effects</i> .....	20
2.3.3 <i>The influence of release direction</i> .....	21
2.3.4 <i>The influence of inclination</i> .....	22
2.3.5 <i>The mixing processes</i> .....	24
2.3.6 <i>Comparison of helium and hydrogen results</i> .....	27
2.3.7 <i>Froude number</i> .....	29
<b>3 Hydrogen ignition .....</b>	<b>31</b>
3.1 Overview of hydrogen ignition .....	31
3.1.1 <i>Flame propagation</i> .....	31
3.2 Experimental setup.....	33
3.2.1 <i>The channel and hydrogen supply</i> .....	33
3.2.2 <i>Ignition and pressure measurements</i> .....	33
3.2.3 <i>Video recording device</i> .....	34
3.3 Results and discussion.....	35
3.3.1 <i>Flame propagation</i> .....	35
3.3.2 <i>Comparison of recorded pressures</i> .....	38
3.3.3 <i>Filled channel scenario</i> .....	40
<b>4 Conclusion .....</b>	<b>43</b>
References .....	45
Appendices .....	47

# Nomenclature

## Abbreviations

BOS	Background Oriented Schlieren
frs	Frame per second
Hysafe	The International Association of Hydrogen Safety
LFL	Low Flammability Limit
MoZEES	Mobility Zero-Emission Energy Systems
SLS	Shadowgraph Lens System
TCL	Telecentric Lenses

## Latin symbols

$D$	diffusion coefficient, [m <sup>2</sup> /s]
$Fr$	Froude number, [-]
$g$	acceleration of gravity, [m/s <sup>2</sup> ]
$h$	height of the mixture cloud, [m]
$h_H$	the height of 100% hydrogen, [m]
$L$	length from channel closed end to the ignition source position, [m]
$l$	characteristic length scale, [m]
$Q$	volumetric flow rate, [m <sup>3</sup> /s]
$Ri$	Richardson number, [-]
$u$	velocity, [m/s]
$u_f$	frontal velocity, [m/s]
$H$	channel height, [m]
$Pe$	Peclet number, [-]
$t$	time, [s]

## Greek symbols

$\rho_1$	density of hydrogen, [kg/m <sup>3</sup> ]
$\rho_2$	density of air, [kg/m <sup>3</sup> ]
$\Delta t$	time of ignition, [s]
$\Delta\rho$	air and hydrogen density difference, [kg/m <sup>3</sup> ]

# 1 Introduction

## 1.1 Background

In recent years, hydrogen has emerged as one of the powerful platforms for energy application and chemical feedstock due to its high energy content and comparatively low environmental effects. There has been an increasing interest in hydrogen as a sustainable energy carrier because of growing concerns about fossil fuel dependence. The global production of hydrogen is gradually increasing in the last ten years. Indeed, it was about 50 million tonnes in 2011 and it reached around 65 million tonnes in 2017 [1, 2]. However, there are several safety hazards associated with hydrogen production, transportation, and utilization. These safety hazards must be considered when treating hydrogen questions and it is very important to carefully examine safety issues connected to hydrogen flammability and explosive properties. Hazards must be evaluated as an outcome from the potential for an accident and the expanse of its consequences. Since 2009 and after the project "Safety of hydrogen as an Energy Carrier", HySafe has terminated, International Association for Hydrogen Safety, IA HySafe is achieved considerable progress in the field of hydrogen safety by coordination between experts in hydrogen safety science and engineering from around the world.

Risks of fire and explosions are central safety considerations connected to the hydrogen application in the transport sector. The hazard of hydrogen explosion is a concern when it leaks in confined spaces such as garages and tunnels. Leak and dispersion of hydrogen in such spaces may result in origination and development of the risky hydrogen-air combustible cloud. Fire safety hazards from the hydrogen-air cloud are determined by the presence of ignition source. Hydrogen dispersion and subsequent explosion of hydrogen-air mixture represent a realistic accident scenario. Therefore, for better development of risk mitigation requirements, it is essential to understand the processes involved during the hydrogen leak, dispersion, and hydrogen-air mixture explosion. Determination of the positions where the cloud could be ignited and the extent to which flame can accelerate depends on the concentration of hydrogen in the combustible cloud [3].

## 1.2 Objective

The specific objective of this thesis was to deepen the degree of understanding in the dispersion of hydrogen focusing in momentum-, buoyancy-controlled jets and the parameters influencing the concentration distribution in confined spaces such as tunnels and channels. There were two primary aims of this study.

First, it was designed to provide a theoretical and experimental analysis of helium and hydrogen dispersion in a confined space by presenting experimental results of measurements and analysis from helium and hydrogen concentration distributions in a laboratory scale three-meter-long channel. Data for this study were collected using concentration sensors at six horizontal positions along the channel and five vertical locations on the channel side at two horizontal sites.

Second, it intended to trace the explosion of the hydrogen-air mixture, subsequent flame evolution when it propagated through the channel and overpressures generated during the combustion process.

### **1.3 Report structure**

This thesis comprises four sections which are divided into subsections and is organized as follows:

The first section gives a brief background and outlines the aim and structure of this document. The second section looks at the question of helium and hydrogen dispersion in a 3 m long channel, and it covers the theoretical bases of dispersion experiments, experimental setup and a subsection involves results and discussions.

section three explores the ignition and explosion of the hydrogen-air mixture in the above-mentioned channel. Overview of hydrogen ignition and flame propagation in confined spaces, description of explosion tests arrangements, and discussions based on experimental results are presented in the included subsections. Conclusions and recommendation for further work are drawn in the final section.

All subsections are divided into subdivisions, and literature studies are joined in the theoretical part of the subsections. Thesis task description, risk evaluation and safety directions of laboratory experiments, and job safety analysis are attached in Appendices A-D. The preliminary draft paper “ Experimental study of light gas dispersion in a channel” which attached in Appendix H is a part of this project and it was written to the International Conference for Hydrogen Safety (ICHS) 2019.

## 2 Hydrogen dispersion

This chapter lays out the theoretical dimensions for the practical analysis of the dispersion of hydrogen in partially-confined spaces. It involves supplemented literature review in sub-chapters of an overview on hydrogen dispersion, helium and its resemblance to hydrogen in the laboratory scale experiments, momentum– and buoyancy-controlled jets, a part of theoretical features of light-fluid intrusion for gravity currents and Froude scaling as a technique used in the researches on tunnel-fire safety.

### 2.1 Overview of hydrogen dispersion

This study addresses hydrogen behavior in confined spaces such as the accumulation, deflagration of hydrogen, and jet-fires in tunnels. The aim is to provide data which can be contributed in closing the knowledge gap in the comprehension of hydrogen dispersion mechanisms and in developing preventive measures to control the accumulation of hydrogen in an enclosure.

Recently, a considerable literature has grown up around the theme of hydrogen dispersion in confined and partially-confined spaces. Investigating hydrogen dispersion is the continuing concern within safety issues relating to hydrogen applications as a transportation fuel. Up to now, several experimental and numerical studies have highlighted conditions and factors associated with hydrogen leaks in confined areas. Gupta et al. [4] have investigated the possible non-catastrophic scenarios related to leakage of hydrogen in a garage and in particular, the influence of hydrogen injected volumes and initial conditions on dispersion and mixing characteristics. The study concluded with that, the flow rate changes have an impact on the mixing behavior inside the garage and subsequently, affect the decay rates of hydrogen concentration. Kyle-Brady et al. [5] have explored the nature of hydrogen dispersion under varied venting conditions by using a two-car garage as a model and platinum foil as a catalytic surface. They suggested that the number and venting arrangements should be estimated depending on potential values of the flow rate to reduce the total amount of hydrogen within an enclosure.

Dispersion and explosion field tests were carried out by Takeno et al. [6], for 40 MPa pressurized hydrogen based on the hypothetical accident scenario of high-pressure pipe's rupture. Concentration measurements were performed, and the results were indicated that hydrogen deflagration is strongly dependent on the turbulent flow after leakage from high-pressure hydrogen gas. Examination of the concentration field and flammability varieties from laboratory scale hydrogen leak was the topic analyzed by De Stefano et al. [7]. During this test, concentration profiles were determined in a model designed like a room in a nuclear facility. Additionally, analysis of the influence of leak location and obstacles presence were performed, and the results pointed out that dispersion was contingent mainly on the flow rate compared to the position of the leak.

A large-scale experimental study was carried out to observe and quantify the creation and development of hydrogen-air flammable cloud in an 80 m<sup>3</sup> chamber constructed inside a rock passage. Detailed examination of the phenomena related to the formation of the explosive mixture and its further possible dissipation due to diffusion by Lacome et al [8] indicated that stratification of the combustible cloud was observed at the upper part of the enclosure for quite

## 2 Hydrogen dispersion

a short duration subsonic releases. The thickness of the hydrogen-air mixture increased with longer release durations, but the concentration observed to be relatively homogeneous and steady.

In follow-up studies, Sommersel et al [9, 10] performed a series of hydrogen release experiments in a 3 m long channel and found that the hydrogen-air cloud flow in the channel can be adequately characterized by Froude scaling obtained from the application of a length scale equal to the height of the layer of 100 % hydrogen. Froude number for hydrogen-air cloud dispersion was estimated to be 0.68 and could be applied for the evaluation of hydrogen leakage in tunnels. Collectively, these studies outline a critical role in understanding the behavior and structure of hydrogen dispersed in a confined space and the factors influencing its development and dissipation.

### 2.1.1 Helium: similarity to hydrogen

There is a potential risk for an unintended explosion when using hydrogen in dispersion tests. Therefore, Helium was selected for a major part of this study due to safety concerns. Helium is considered to resemble hydrogen since it has analogous low density and high buoyancy. Helium is twice dense as hydrogen and they have about 8% difference in buoyancies. Molecular diffusion coefficient of helium is about 90% of that for hydrogen. Helium and hydrogen volumetric flow rates were assumed to be equal in the prediction of hydrogen dispersion and explosion using helium. However, several studies were mentioned the difference between helium and hydrogen flow rates between helium and hydrogen flow rates [11-14]. To use precisely helium as hydrogen simulant, Jiaqing He et al [11] suggested that differences in air-helium and air-hydrogen densities should be considered in the relationship between the volumetric flow rate of helium and hydrogen.

### 2.1.2 Momentum- and buoyancy-controlled jets

There are three types of released jets depending on the effect of buoyancy. Momentum-controlled, buoyancy-controlled which are fast redirected to vertical flow, and transitional which have momentum-controlled jet nearer to release point and buoyancy-controlled downstream. The hydrogen gas released in a channel will disperse by diffusive and buoyant forces. The influence of buoyancy on the gas wave is more significant than diffusivity at low-momentum hydrogen releases[15]. Therefore, highly concentrated with hydrogen and less dense gas cloud rises close to release point and the variation in densities promotes buoyancy forces which cause the cloud to upsurge vertically and proceeds at the upper part of the channel. Thereafter, the hydrogen-rich cloud loses its inertia gradually and becomes buoyancy-driven. The mixing process with air either in the formation of the cloud or when the cloud propagates downstream occurs in nonhomogeneous mode. Thus, concentration decays along the jet axis and horizontally away from the release site[16].

### 2.1.3 Gravity Currents

Gravity currents generated in the horizontal flows due to density differences in the fluid under a gravitational field. An important kind of gravity currents is a flow of less dense gas caused by the accidental release in tunnels or other semi-confined spaces. Density variations in a gravitational field generate buoyancy forces which cause the flow into horizontal motion and

## 2 Hydrogen dispersion

produce horizontal pressure gradients. The front zone formed by a gravity current is characterized by the presence of a sharp line dividing the two fluids. The front shape of the cloud formed by a gravity current is affected by the opposite ambient flow [17]. Turbulent mixing typically occurs at gravity current front and the mixing process continues at the interface between the two fluids as the cloud spreads. According to J. E. Simpson analysis [17], three regions are observed at the front of gravity current, the upper layer where the less dense cloud is moving, bottom layer with air and the mixing region between these two layers. Figure 2.1 illustrates the front and the three regions with their conforming heights.

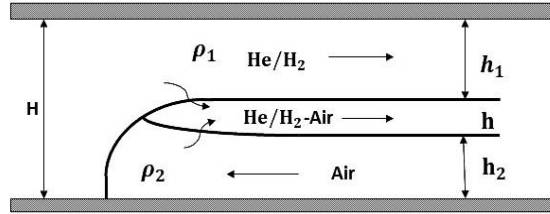


Figure 2.1: A mixing region at the front of a gravity current

### 2.1.4 Froude scaling

Scaling techniques are extensively applied in researches of tunnel fire safety, and the major preserved dimensionless group in these researches is the Froude number. The dimensionless Froude number is the ratio between inertia and gravity forces exerting influence on the fluid flow and it can be used to describe the dispersion of hydrogen/helium in a channel [18]. Froude number is related to the front velocity of a gravity current as

$$Fr = u/\sqrt{gl} \quad (2.1)$$

where  $u$  is the velocity,  $g$  is the acceleration due to gravity, and  $l$  is a length scale.

Figure 2.2 represents the shape of the pre-mixed cloud as it propagates after the gas injection into the channel.

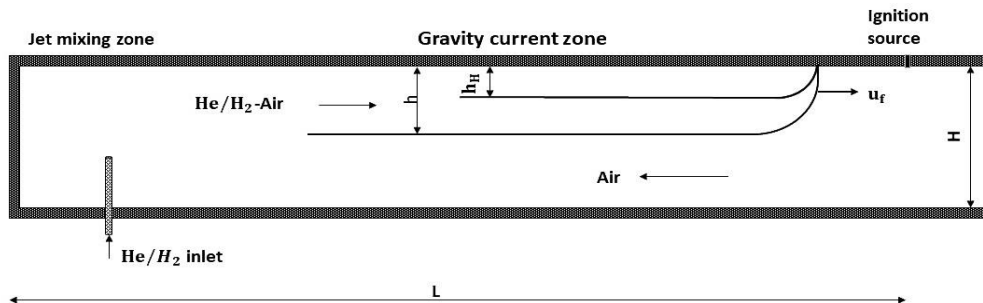


Figure 2.2: Schematic illustration of hydrogen/helium-air cloud formed by gravity current in the channel

The front velocity of the cloud in the channel is  $u_f$ , and the characteristic length scale,  $l$ , can be represented as the theoretical layer of 100% hydrogen/helium,  $h_H$ . The reason for this option

## 2 Hydrogen dispersion

is that the front velocity is not affected by the mutual intrusion in dispersion process since the increase in the height of the cloud depends on the hydrogen/ helium flow rate and balanced by the decrease in cloud density [9, 19]. The gas flow rate into the channel,  $Q$  [ $\text{m}^3/\text{s}$ ] can be connected to the unmixed layer,  $h_H$ , as

$$Q = u_f \cdot h_H \cdot w \quad (2.2)$$

where  $w$  is the width of the channel. Substitution of the unmixed layer,  $h_H$ , in the Froude number expression, gives

$$Fr = \sqrt{u_f^3 \cdot w/gQ} \quad (2.3)$$

The average cloud front velocity,  $u_f$ , can be expressed in terms of the distance covered by the cloud from the release point to reach the sensor's position (or ignition point),  $L$  [m], and the time required to reach this point,  $\Delta t$  [s]. thus, Froude number can be rewritten as

$$Fr = \sqrt{\left(\frac{L}{\Delta t}\right)^3 \cdot w/gQ} \quad (2.4)$$

Richardson number expresses the ratio of buoyancy expression to the flow shear expression and it is correlated to Froude number by rearranging the formula 2.1 as

$$Fr^2 = \rho u^2 / \Delta \rho g h = Ri^{-1} \quad (2.5)$$



## 2.2 Experimental setup

This section describes channel setup, measurement devices and the flow imaging systems used to perform hydrogen dispersion experiments besides experimental models.

### 2.2.1 Channel description

Experiments were executed in a horizontal rectangular cuboid channel with dimensions: 3 m length, 0.1 m width, and height. The channel was made of coated steel with transparent polycarbonate sidewalls. It was open on one side and closed in the other. The volume of the channel was  $0.03 \text{ m}^3$ . Figure 2.3 presents a schematic design of the channel and indicating the positions of concentration measurement sensors. Figure 2.4 shows an oblique image of it.

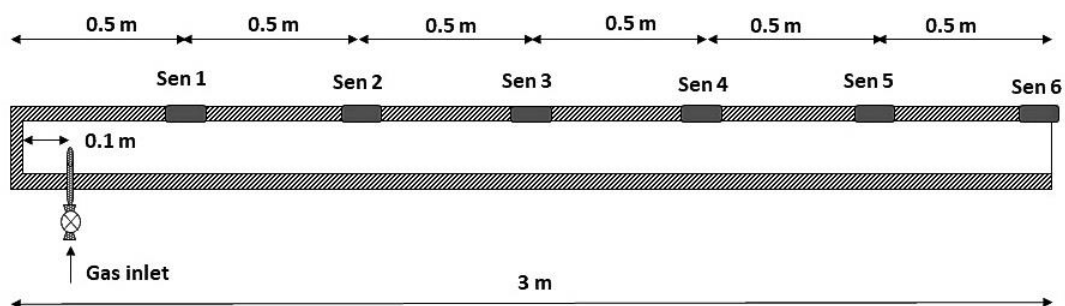


Figure 2.3: Schematic design of the channel with sensors positions



Figure 2.4: An oblique image of the channel setup

### 2.2.2 Helium and hydrogen injection

Helium was provided from helium standard 180 bar cylinder and hydrogen from a standard 200 bar cylinder. The gas flow was adjusted by Purgemaster volume flow meter with releasing flow rate in the range of 5 to 90  $\text{Ndm}^3/\text{min}$ . The flow meter was calibrated before measurements start by Ritter drum-type TG 10/1. Then the gas was injected into the channel upwards or downwards through a 4 mm pipe, which located at centerline 100 mm from the closed end and had 50 mm height in the channel. Besides the inlet 4 mm pipe, different circular nozzles with diameters 2.5, 1 and 0.5 mm were used for injection of helium into the channel. Figure 2.5 shows the three nozzle sizes used in the tests.

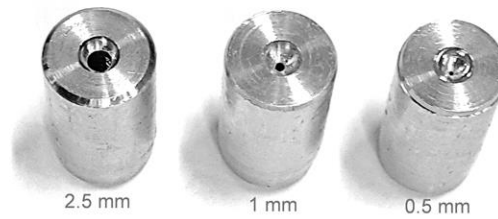


Figure 2.5: Different sizes of circular nozzles used in the experiments

### 2.2.3 Measurement devices

Measurement of helium concentration as volume percentage was recorded by XEN-5320 gas sensor for determining gas composition Figure 2.6. The XEN-5320 is an integrated sensor based on the measurement of the thermal conductivity of the gas. It automatically makes a correction to temperature and humidity measurements to compensate for their influence. The sensor was WIFI read out, connected to a special WIFI network for measurements in the laboratory and it sent the measurements to a specific computer program (Xen-5320 LabView Standard v3.20 WIFI). Sensors were located at six different positions along the channel. The first one was located 0.4 m from the release point, and the others were positioned 0.5 m from each other (Figure 2.3).



Figure 2.6: Concentration sensors XEN-5320 from Xensor Integration. WIFI read out.

Helium volume fractions were similarly recorded at five vertical positions, at 10, 30, 50, 70 and 90 mm from the ceiling, at the horizontal location, 2.5 and 3 m from the channel closed end. Figure 2.7 lustrates the vertical sensor's positions at two horizontal sites.

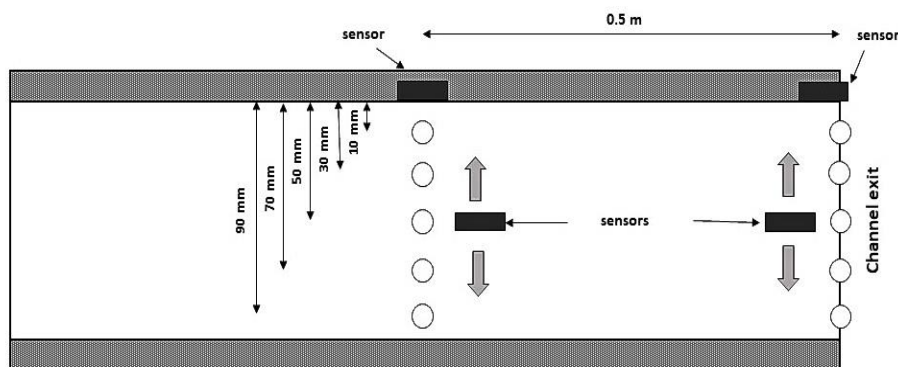


Figure 2.7: Sensors positions for measuring He concentration at the different vertical location at 500 mm from the channel exit and at the exit.

## 2.2.4 Flow visualization techniques

Flow imaging systems provide a technique to visualize changes in refractive index depending on the density variation of transparent media [20]. Two systems were used in this study, Background-Oriented Schlieren (BOS) and Shadowgraph lens system (SLS).

Background-Oriented Schlieren was used for imaging the helium release and dispersion in the mixing zone of the channel. Typical BOS system involves appropriate patterned background, a camera and a computer for post-processing [20]. Figure 2.8 shows a representative drawing of the BOS arrangement. It is possible to identify refractive index deflections by comparing undistorted background image with distorted by flow refractions background, then implementing computer processing to estimate density gradients [21].

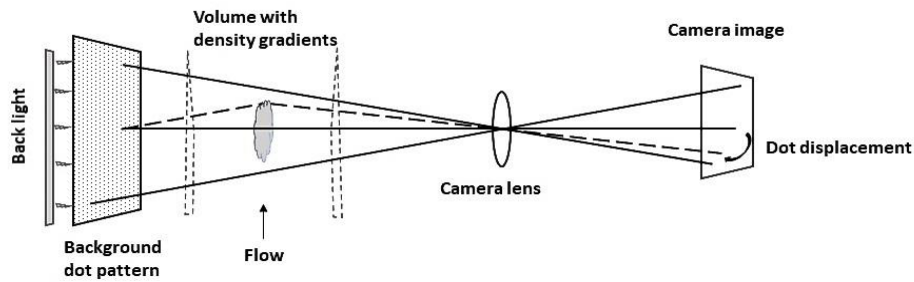


Figure 2.8: Conceptual drawing of Background-Oriented Schlieren (BOS)

To improve contrast and readability, a backlit background with dot pattern was composed behind the channel. Photron SA1.1 high-speed video camera was operated as a recording device. The camera fitted out with Nikon ED lens (AF NIKKOR 80-200 mm 1:2.8 D) and controlled by computer software: Photron FastCam viewer (ver. 3670).

Shadowgraph system was utilized to visualize the air-helium cloud formation next to the release point and the shape of the cloud, once it propagated through the lenses located at 1.5 m from the channel closed end. The system includes lenses from OPTO ENGINEERING, Telecentric TC lenses, and LTCLHP high-performance illuminator to illuminate objects imaged by Telecentric lenses. The lenses were fixed to a slab with clamps. FastCam APX RS camera was linked to the lenses for image recording. Figure 2.9 presents the drawing of a shadowgraph system and Figure 2.10 show the image of the system fixed in the middle of the channel.

In shadowgram, the tendency of light rays to converge depends on the density gradient, and illumination variations in the picture are proportional to the second derivative of the density. This implies that the shadowgraph gives best results for flow fields with the swift difference in density gradients. The increase in light intensity for 2-D flow can be expressed as follows

$$\Delta I = k \left( \frac{\partial^2 \rho}{\partial^2 x} + \frac{\partial^2 \rho}{\partial^2 y} \right) \quad (2.6)$$

where  $k$  is constant,  $x$  and  $y$  are coordinates on the plane normal to the light path [22].

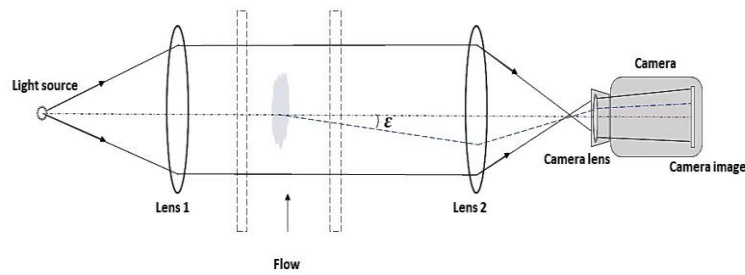


Figure 2.9: A drawing depicts a shadowgraph system



Figure 2.10: The configuration of Shadowgraph system used in the experiments

### 2.2.5 Experimental models

Different sets of experiments were performed to investigate the influence of various parameters on the helium concentration distribution in the channel. Parameters include flow rate, nozzle size, concentration vertical distribution, injection direction, and channel inclination. All parameters in the process interact, therefore, concentration measurements were divided into three models, horizontal and vertical concentration distribution, in addition to inclined channel measurements.

Horizontal measurements involve recording the concentration by sensors along the channel, as it can be seen in Figure 2.3, for different flow rates, nozzle size and release directions, upward, U, and downwards, D. Table 3.1 gives an overview of the horizontal measurement's matrix.

Table 2.1: The first model experimental matrix.

Flow rate, Ndm <sup>3</sup> /min	Nozzle size							
	0.5 mm		1 mm		2.5 mm		pipe 4 mm	
5	U	D			U	D	U	
15	U	D			U	D	U	
40	U	D	U	D	U	D	U	D

The second model is the concentration measurements vertically at two locations on the channel, 2.5 m from the channel closed end and at the exit. Sensor's positions were 0, 10, 30, 50, 70 and 90 mm from the ceiling as presented in Figure 2.7. Table 3.2 defines the parameters during the measurements.

Table 2.2: experimental model for vertical concentration distribution.

Parameter	Nozzle size	
	1 mm	Pipe 4 mm
Flow rate, Ndm <sup>3</sup> /min	5, 15 and 40	40
Release direction	downward	upward and downward
Position, m (from the channel end)	2.5 and 3	2.5 and 3

The third model is the determination of helium concentration lengthways the inclined channel. Measurements were done for channel inclination of 10 and -10 degrees. Figure 2.11 illustrates a drawing of an inclined channel towards the exit (-10 degrees).

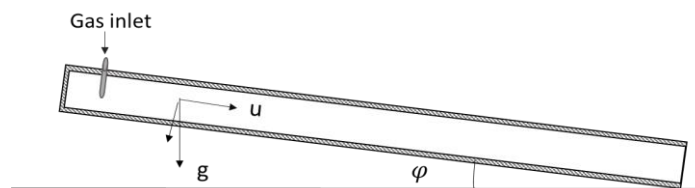


Figure 2.11: inclined channel at -10°(towards the exit)

Helium released downward at flow rates 15 and 40 dm<sup>3</sup>/min through a pipe diameter 4 mm.

All the experiments were implemented at ambient temperature and pressure during the release time of 3 minutes.

The fourth model covered the measurements of helium and hydrogen concentrations as it explained in the helium horizontal model with the same parameters in Table 1. In this model Swagelok pneumatic valve connected to the inlet pipe for better control of the gas flow rate. The pneumatic valve was triggered together with a pressure sensor to record the pressure at the valve during the gas release. Additional information about devices is given in Appendix G.

## 2.3 Results and discussions

### 2.3.1 Flow rate effects

Results from the sensor's measurements for helium concentration along the channel at flow rates 5, 15 and 40  $\text{Ndm}^3/\text{min}$  and 3 minutes release time are shown in Figure 2.12. The figure displays a clear increase in helium concentration recorded by sensors at all measurements locations with an increase in the flow rate. Simultaneously, the time between the sensor's recording starts decreases. This indicates a rise in the cloud's velocity with an increase in flow rates.

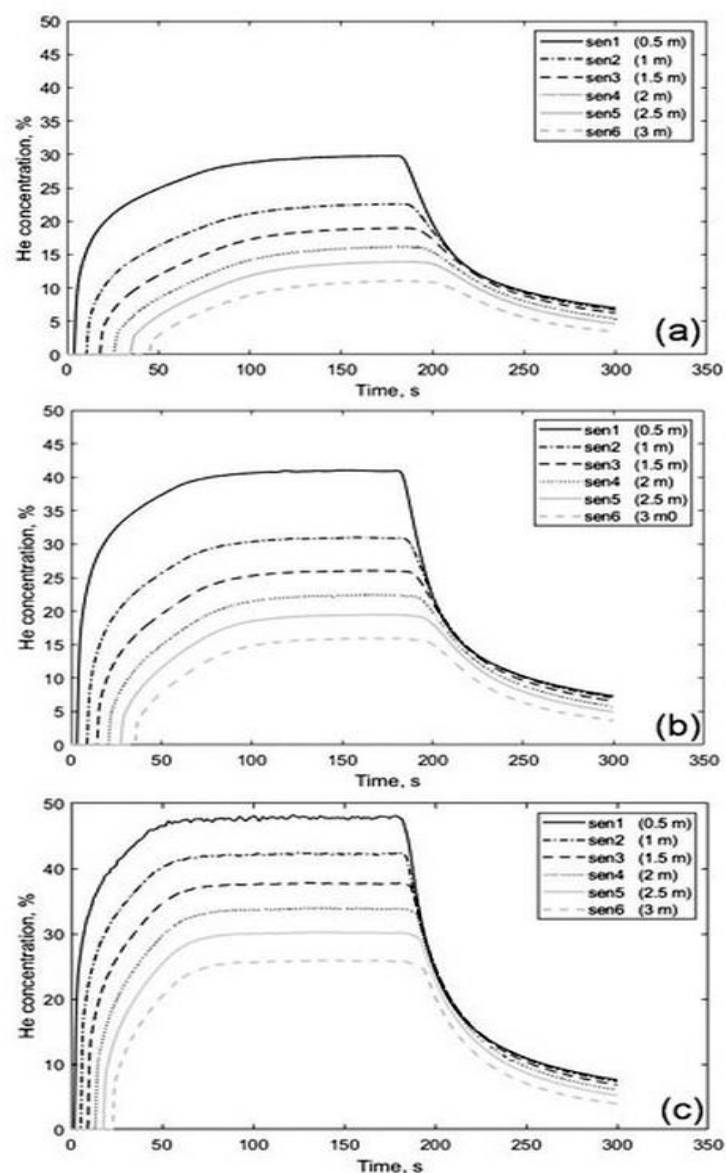


Figure 2.12: Helium output concentration over time for upward release through 4 mm diameter pipe and at flow rates: (a) 5, (b) 15 and (c) 40  $\text{Ndm}^3/\text{min}$

## 2 Hydrogen dispersion

Concentration's decay lengthways the channel signifies that helium-air cloud loses its inertia while it propagates through the channel and turns to be buoyancy-driven. This process decays with an increase in the flow rate as can be seen from (a) to (c) graphs in Figure 2.12.

The vertical concentration distribution of helium in the channel was determined by recording the concentration in two horizontal positions, at 2.5 m from the channel closed end and the channel exit. Vertical positions were 0,10, 30, 50, 70, 90 mm from the channel ceiling. Figure 2.13 shows helium output concentration as the function of time at cited vertical locations for downward release through 2.5 mm nozzle and at 2.5 m from the closed end.

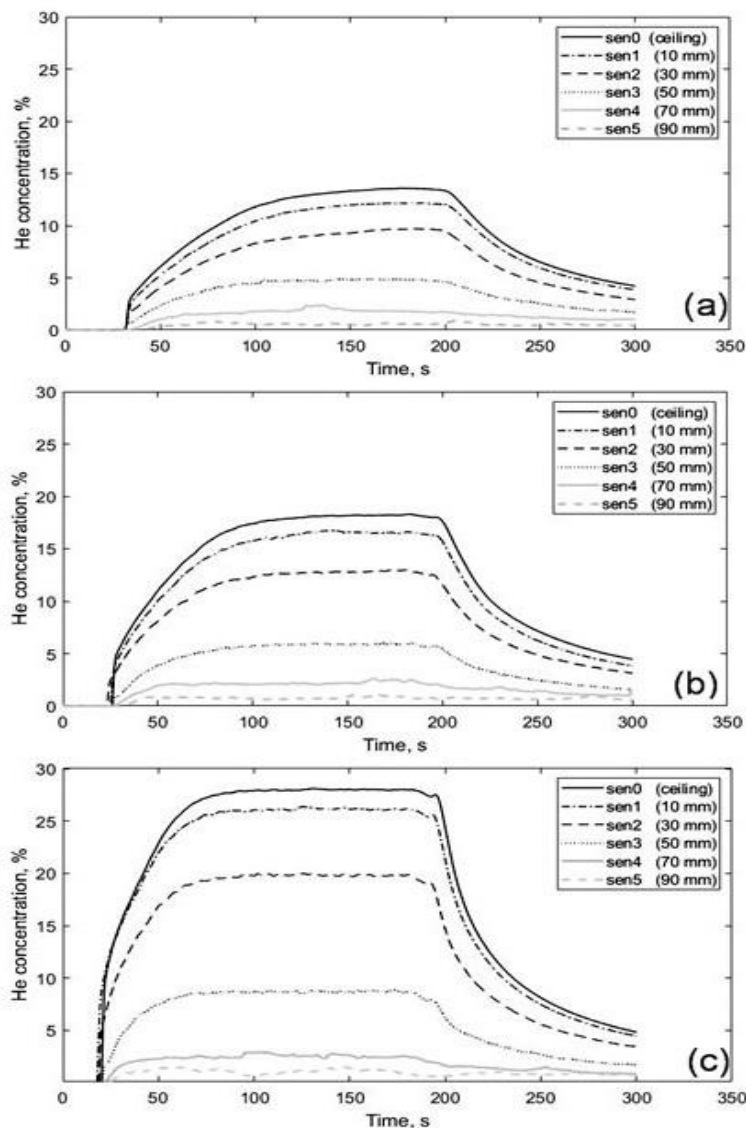


Figure 2.13: Distribution of helium concentration vertically over time for downward release through 2.5 mm nozzle size and at flow rates: (a) 5, (b) 15 and (c) 40  $\text{Ndm}^3/\text{min}$ .

Over-all constructed concentration profiles with different flow rates were observed unchanged. Helium concentration moved upward close to the ceiling from 13.8 % in (a) to 28.2 % in (c) while the flow rate was raised up from 5 in (a) to 40  $\text{Ndm}^3/\text{min}$  in (c) graphs in Figure 2.13.



## 2 Hydrogen dispersion

This indicates that concentration decays horizontally and vertically while the cloud is propagating in the channel.

### 2.3.2 Nozzle size effects

Sensors measurements for helium dispersal in the channel were done using different nozzle sizes, 0.5, 1, 2.5 mm and pipe diameter 4mm. Figure 2.14 illustrates helium concentration over a period of 5 minutes for downward release at  $40 \text{ Ndm}^3/\text{min}$  for four defined nozzle sizes. As evident from the graphs in Figure 2.14, the upper lines are becoming more undulate and the differences between two upper concentration lines decrease from 1.86% in the graph (d) to 1.15% in the graph (a), with a decrease in nozzle size, from 4 to 0.5 mm. This specifies more rapid mixing of helium with air occurs close to the release point due to the rise in flow velocity as the nozzle size decreases. It can also be observed from the time that lines are level out, 87s in the graph (a) to 71s in (d).

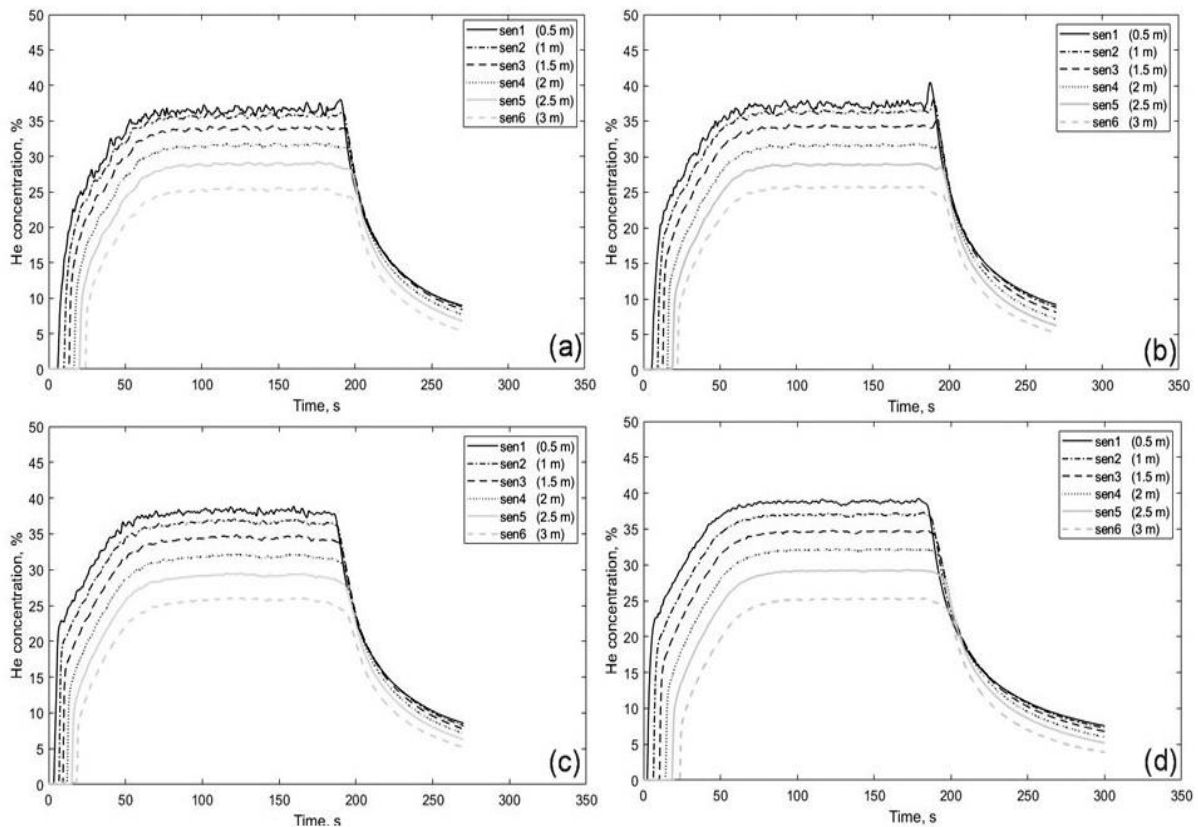


Figure 2.14: Output concentration over time of helium downward release at  $40 \text{ Ndm}^3/\text{min}$  and through nozzle sizes: (a) 0.5, (b) 1, (c) 2.5 mm and (d) pipe diameter 4 mm.

Figure 2.15 demonstrates helium concentration vertical measurements for 3 minutes downward release at a flow rate of  $40 \text{ Ndm}^3/\text{min}$  through 2.5 mm nozzle size and 4 mm pipe. The trends presented in this figure are like those in Figure 2.13. The concentration slightly increased with nozzle size has been changed from 2.5 mm to 4 mm. simultaneously, the difference between the two upper sensor's readings line increased. This may be explained by the concentration drop as the mixing process developed faster with a smaller nozzle size.



## 2 Hydrogen dispersion

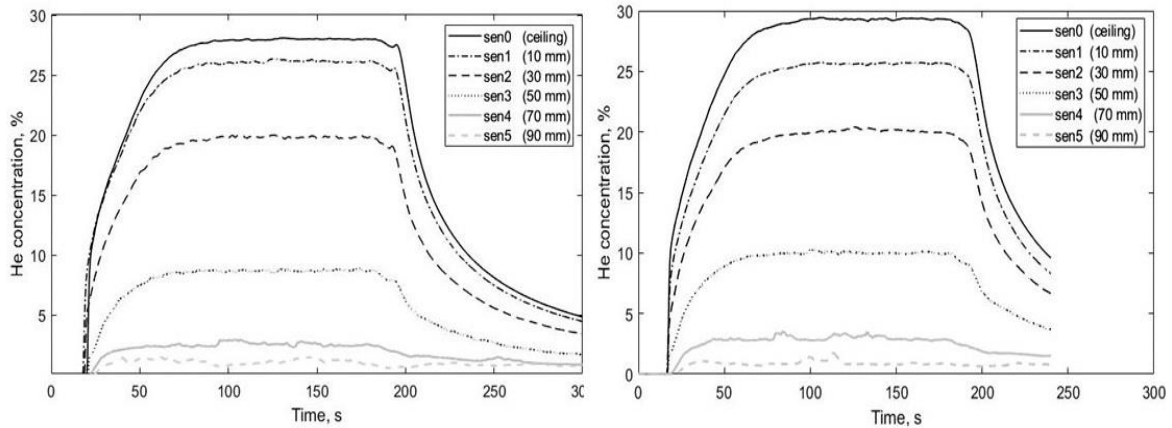


Figure 2.15: Vertical concentration distribution over time of helium downward release at  $40 \text{ Ndm}^3/\text{min}$  and through nozzle sizes, 2.5 mm (left) and pipe diameter 4 mm (right).

### 2.3.3 The influence of release direction

The changes in helium concentration distribution were identified by helium upward and downward injections at different flow rates and nozzle sizes. Figure 2.16 demonstrates helium concentration over time for releases through a 2.5 mm nozzle size and at a flow rate of  $15 \text{ Ndm}^3/\text{min}$ . It is apparent from the graphs presented in Figure 2.16 that the concentration recorded by the first sensor is higher for upward release than for downward. This happened because of the mixing process is higher near the release point and mainly induced by momentum. Formed mixture by downward release changes direction upwards due to density difference and mixes additionally with air while it proceeds downstream occupying the upper part of the channel.

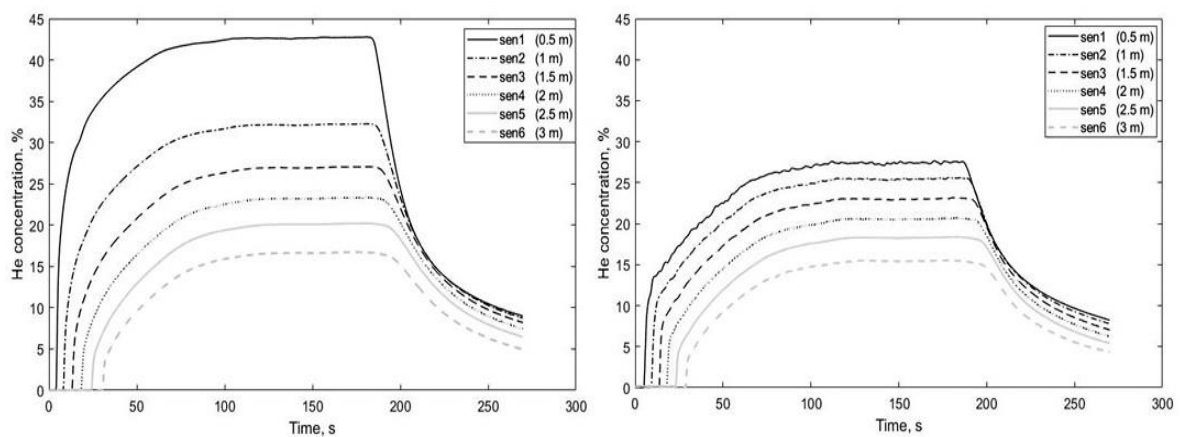


Figure 2.16: Output helium concentration versus time for upward release, left and downward, right at flow rate  $15 \text{ Ndm}^3/\text{min}$  and 2.5 mm nozzle size.

## 2 Hydrogen dispersion

Figure 2.17 shows the vertical helium concentration distribution for upward release, on the left-hand side and downward, right at a flow rate of  $40 \text{ Ndm}^3/\text{min}$ . No differences in vertical distribution have been observed between upward and downward releases away from the release point. The reason for this is likely to be related to the fact that the mixing is mainly buoyancy driven process while the cloud propagating away from the release point.

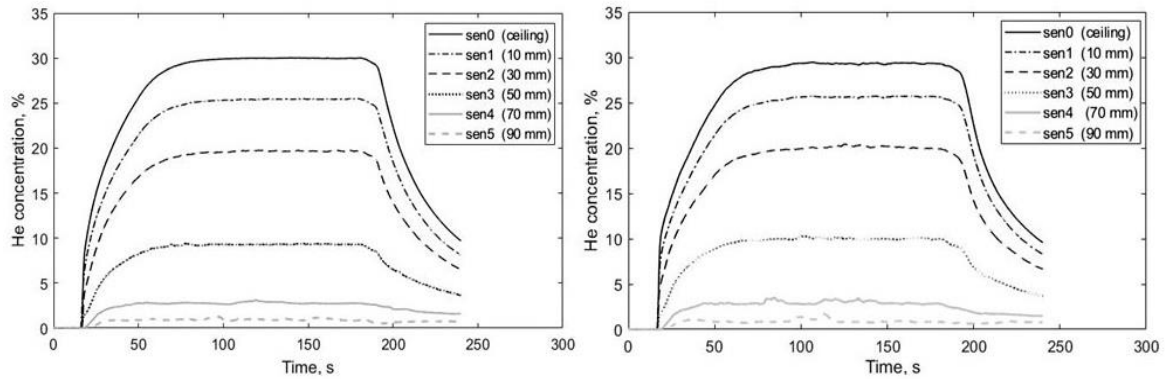


Figure 2.17: Vertical helium concentration distribution over time for upward release, left and downward, right at a flow rate  $40 \text{ Ndm}^3/\text{min}$  and through a pipe diameter 4mm.

### 2.3.4 The influence of inclination

The channel was inclined by 10 and -10 degrees in order to analyse how the inclination affect concentration distribution in the channel. Helium was released downward through 4 mm pipe at 15 and  $40 \text{ Ndm}^3/\text{min}$ . Descriptive data were generated for all sensor's positions depicting dissimilarity of the two tilted channel structures. Figure 2.18 displays helium concentration over time for downward releases in the inclined channel by 10 degrees, left and -10 degrees, right at  $15 \text{ Ndm}^3/\text{min}$ .

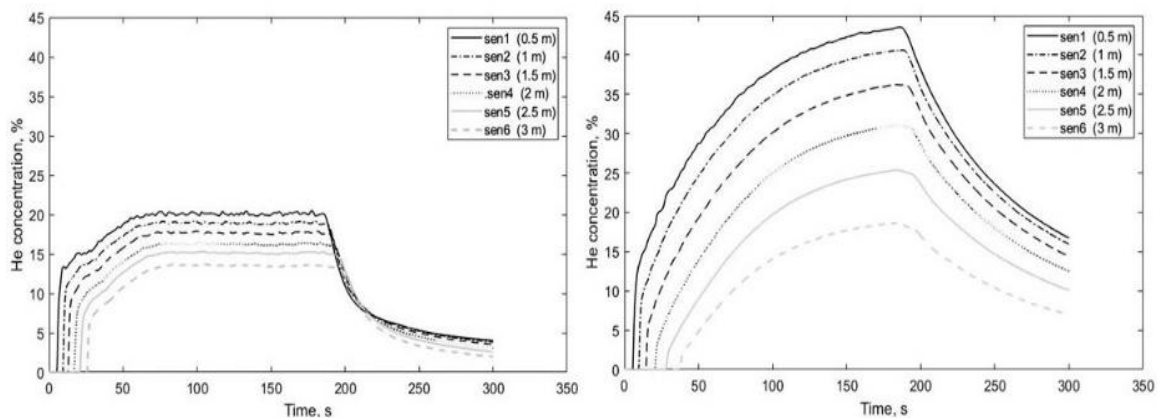


Figure 2.18: Helium concentration over time for downward release in the channel with an inclination of  $10^\circ$ , left and  $-10^\circ$ , right at  $15 \text{ Ndm}^3/\text{min}$  and through 4 mm pipe.

From the data in the above graphs, it is apparent that helium concentration is swiftly rising and reach much higher levels in an inclined channel by  $-10^\circ$  than by  $10^\circ$ . Furthermore, the concentration lines are situated closer to each other for the channel with positive inclination,

## 2 Hydrogen dispersion

on the left side, than with negative inclination, right. The observed differences in concentration gradients could be attributed to the rapid mixing process in the positive channel inclination. In the channel with negative inclination, the air inflows and mixes with helium is affected by the gravity leading up to a reduction in the mixing intensity and growth of the cloud leading-front propagation rate. This outcome can be well observed comparing positive and negative channel inclination with horizontal channel position. Figure 2.19 compares helium concentration distribution in an inclined channel by  $10^\circ$ , horizontal channel and inclined channel by  $-10^\circ$ .

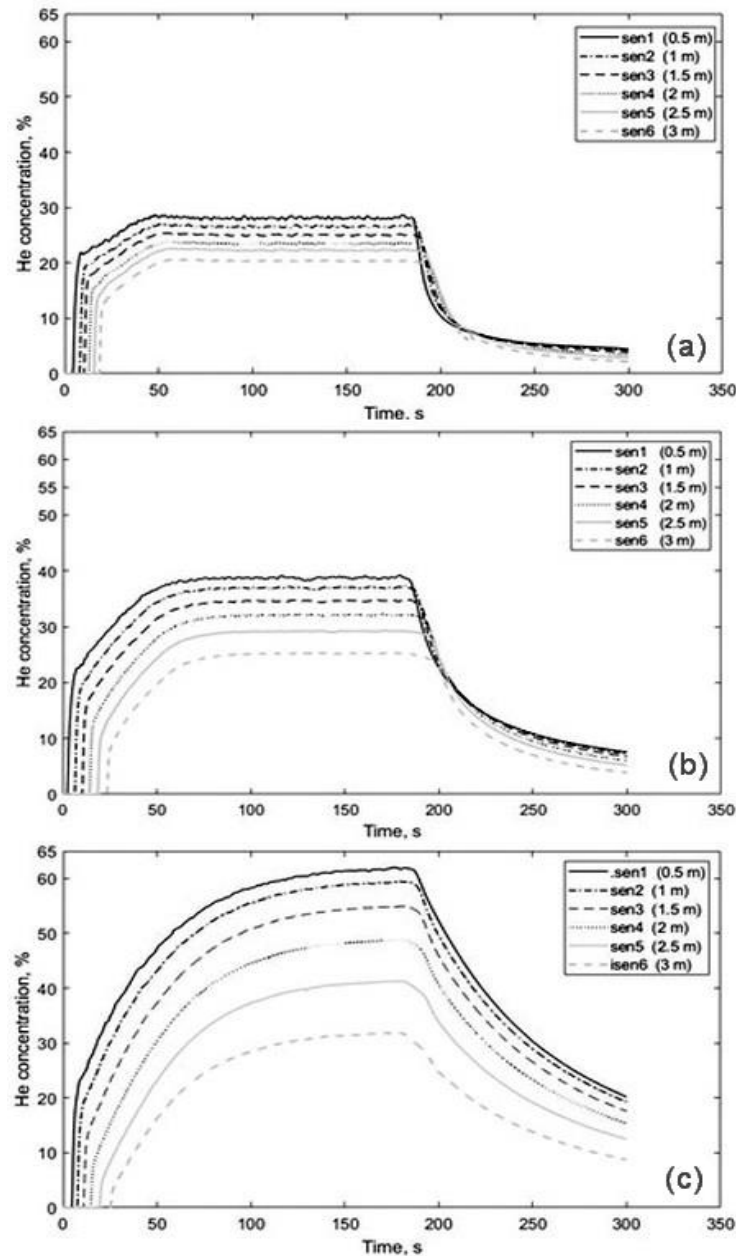


Figure 2.19: Helium concentration over time for downward release through 4 mm pipe at  $40 \text{ Ndm}^3/\text{min}$  and in the channel with an inclination of  $10^\circ$ , left, horizontal, middle and inclination of  $-10^\circ$ , right.

For the purpose of a detailed comparison of the concentration profiles and quantities, concentration read-out from the first sensor in the horizontal and inclined channel by  $-10^\circ$  and  $10^\circ$  is presented in Figure 2.20

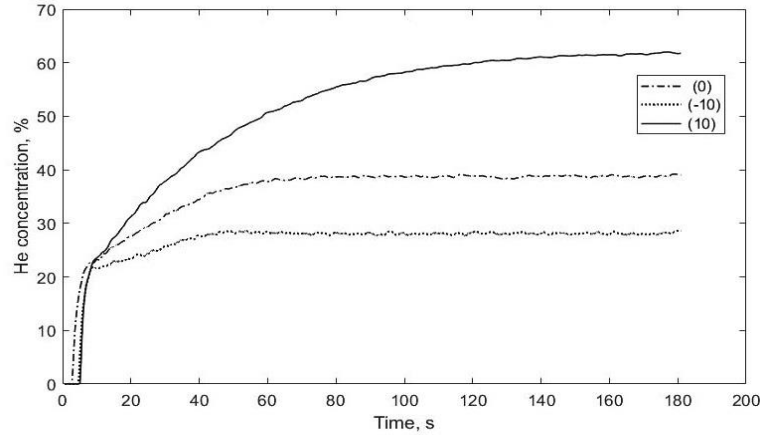


Figure 2.20: helium concentration over time recorded at the first sensor, 0.5 m from the channel closed end for downward release at a flow rate of  $40 \text{ Ndm}^3/\text{min}$ , through 4 mm pipe, and for channel inclination of  $-10^\circ, 0^\circ$ , and  $10^\circ$ .

### 2.3.5 The mixing processes

In a case of helium downward release in the channel, the mixing processes occur rapidly, and the created concentration pattern is basically depending on the radial and axial direction relevant to injection pipe and correspondingly on the horizontal and vertical axis of the channel. The upward flow of the helium-air mixture is fast and the propagation velocity of the mixture cloud is contingent on the flow rate of helium. Furthermore, the mixing processes around the injection pipe are both momentum-driven and buoyancy-driven, but mainly buoyancy-driven away from the release point.

Distribution of helium molecules could be driven by molecular diffusion. Correlation between advective and diffusive mixing may be obtained from the general advection-diffusion transport equation by representation in terms of non-dimensional Peclet number. The significance of advection and diffusion in the mixing process could be estimated from the following relation

$$Pe = D/u^2 \cdot t = D/u \cdot l \quad (2.7)$$

Where  $D$  is species diffusivity,  $u$  is flow velocity,  $t$  is the time and  $l$  is a characteristic length scale

The Peclet number denotes the ratio between the characteristic times of advection and diffusion and if  $Pe \gg 1$ , the transport is diffusion dominant, if  $Pe \ll 1$  then the process is dominating by advection.

Results from the calculation of Peclet number at a flow rate ranging from 90 to 5  $\text{Ndm}^3/\text{min}$ , through pipe diameter 4 mm and at different positions in the channel show that  $Pe$  is ranging between  $1.09 \cdot 10^{-4}$  and  $11.93 \cdot 10^{-4}$ . These numbers are much lesser than 1, this implies the mixing process is advection dominant and molecular diffusion can be neglected.

## 2 Hydrogen dispersion

As expected, the results of the experiments show that helium mixes with air more rapidly at higher flow rates, smaller nozzle sizes, and downward release direction. Dispersion of helium in the channel characterized by the formation of inhomogeneous and stratified cloud. The mixing phenomena primarily start rapidly near the injection pipe and can be described as jet momentum-induced mixing. The cloud is developed around the injection pipe with high helium concentration and less dense mixture than air. Subsequently, the cloud starts to rise up due to buoyancy induced by density difference. Buoyancy-induced mixing continues as the cloud propagates through the channel creating a mixing zone as a line dividing the two fluids. In an attempt to visualize described phenomena, Background-oriented Schlieren and shadowgraph lens system were performed as defined in section (2.4).

Figure 2.21 represents images of mixing development around the release pipe captured by means of Background-oriented Schlieren for downward helium release at a flow rate of 40 Ndm<sup>3</sup>/min through 4 mm pipe. The mixing process begins at the initiated helium-air interface and then gradually expands vertically and horizontally creating a positive concentration gradient for helium in the upward direction. This implies that the highest helium concentration is at the ceiling. The change in concentration pattern is more considerable on the horizontal direction and this because of, firstly, the movement of helium-air cloud behaves as a gravity current and, secondly, the concentration decays while the cloud propagating along the channel. Regardless of the images' quality, they clearly show the formation of the cloud and the mixing zones represented as bright layers which are corresponding the theoretical lines divided the two fluids.

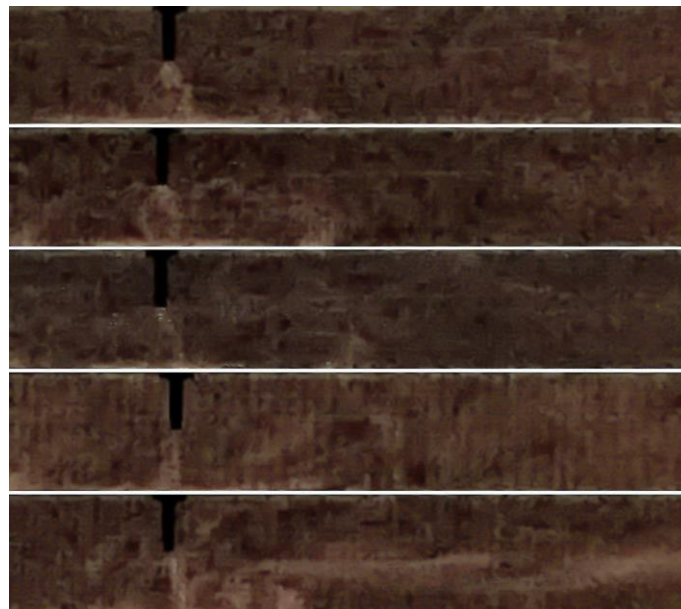


Figure 2.21: The mixing process following Helium downward releases through 4 mm pipe at 40 Ndm<sup>3</sup>/min visualized by Background-oriented Schlieren technique for 10 s.

Figure 2.22 demonstrates shadowgrams of concentration gradients at the upper part of the channel after helium release at a flow rate of 50 Ndm<sup>3</sup>/min for 5.4 seconds.

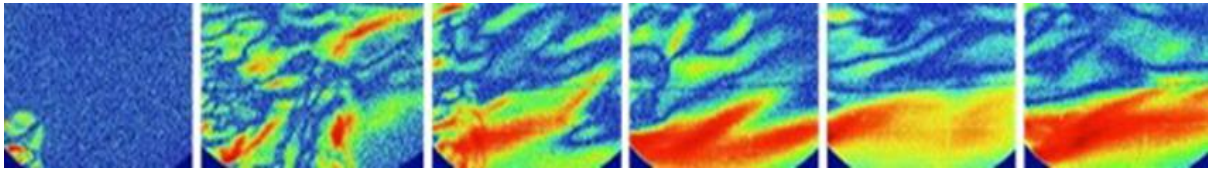


Figure 2.22: Helium concentration gradients next to the release point visualized by shadowgraph for downward release at  $50 \text{ Ndm}^3/\text{min}$  through pipe diameter 4 mm.

Above images designate a complex mode of mixing flow pattern next to injection pipe and indicate how the mixing zone develops from breakage into multiple fragments with a narrow region on the interface between helium and air, to rapidly emerging of thin layers which are further becoming wider. Images show evidently the developing of mixing zone to form a layer divided the two fluids as specified in the gravity currents theory in section (1.3). Furthermore, they also express the inhomogeneous and stratified nature of the helium-air cloud while it propagates in the channel.

### 2.3.6 Comparison of helium and hydrogen results

Measurements of hydrogen and helium concentration along the channel were performed for 3 minutes release time through pipe diameter 4 mm and flow rates, 5, 15 and 40  $\text{Ndm}^3/\text{min}$ . the results of these measurements are shown in Figure 2.23 and Figure 2.24 Hydrogen concentration is higher from (a) to (c) graphs in Figure 2.23 compared with corresponding graphs for helium in Figure 2.24 These results are likely to be related to the differences in density hydrogen/air and helium/air which has been reported by Jiaqing He et al [2].

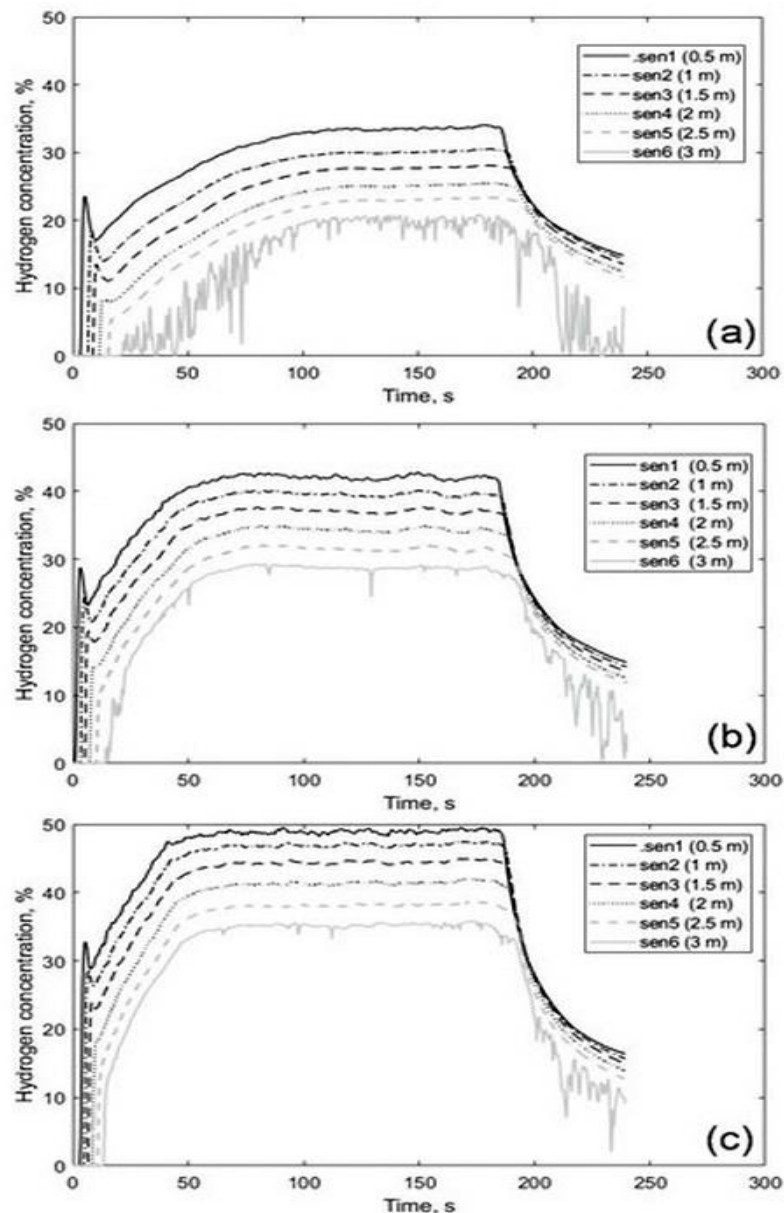


Figure 2.23: Hydrogen concentration over time for downward releases at flow rates, 5 (a), 15 (b) and 40  $\text{Ndm}^3/\text{min}$  (c), through pipe diameter 4 mm.

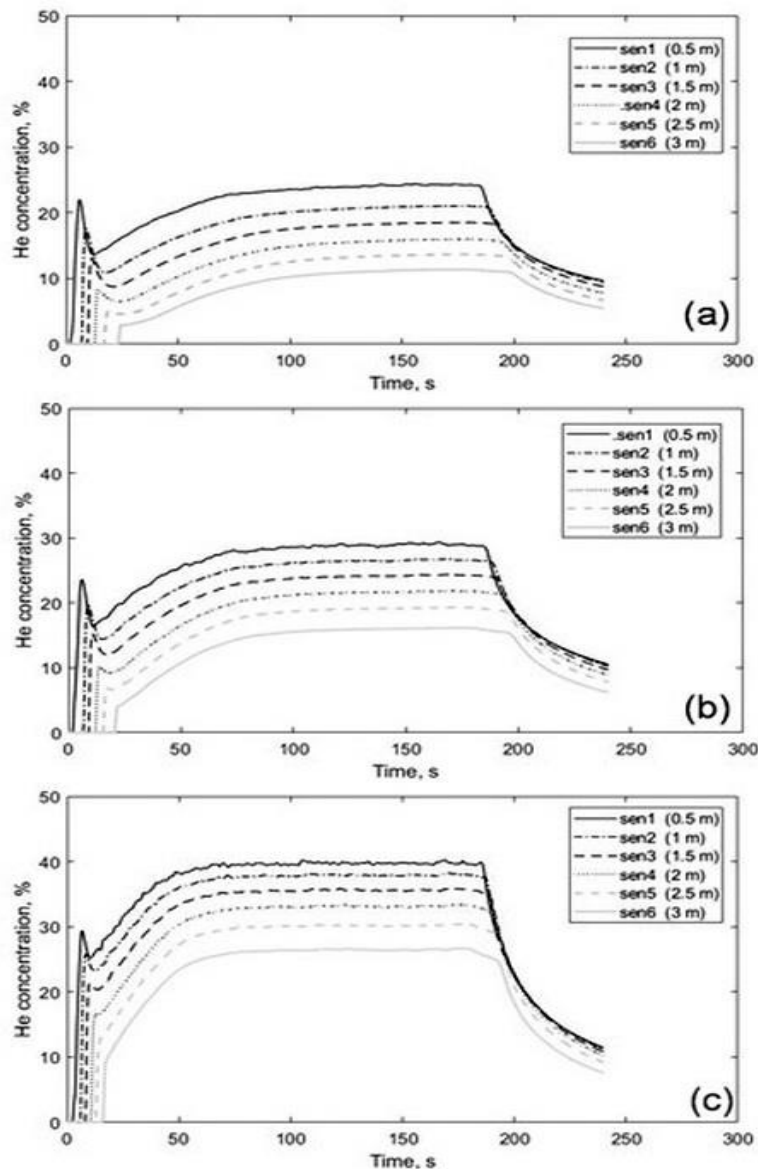


Figure 2.24: Helium concentration over time for downward releases through 4 mm pipe at flow rates, 5 (a), 15 (b) and 40  $\text{Ndm}^3/\text{min}$  (c).

Comparing hydrogen and helium releases at a low flow rate, graphs (a) in Figure 2.23 and Figure 2.24, the hydrogen concentration is slightly higher than that for helium, but they behave differently at the channel exit. The lowest concentration line for hydrogen in Figure 2.23 is rippling, which denotes higher mixing of the hydrogen-air cloud with air at the channel exit than for helium-air cloud. The leap up which appears at the beginning of measurements is likely to be related to the change in pressure at the pneumatic valve and simultaneously the entering of the gas volume in the tube to the channel through the valve. (graphs pressure-time at the pneumatic valve are given in Appendix E.)

A comparison of the shape and front velocity of the hydrogen-air cloud and the helium-air cloud was drawn by implementing the shadowgraph technique as described in section (2.4) at the middle of the channel, 1.5 m from the closed end and the results are shown in Figure 2.25.



## 2 Hydrogen dispersion

Hydrogen and helium were Released downward through 4 mm pipe at a flow rate of 40 Ndm<sup>3</sup>/min.

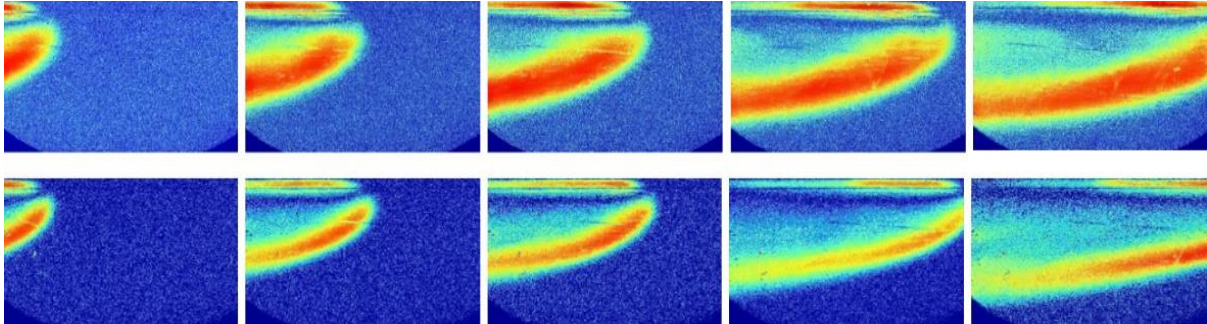


Figure 2.25: Concentration gradients of helium, upper series, and hydrogen, lower series, visualized by shadowgraph while the cloud propagating through the channel for at 1.5 m from the channel closed end for downward releases through 4 mm pipe and flow rate 40 Ndm<sup>3</sup>/min.

The most interesting aspect of these images is the thickness of the mixing zone, which represents the higher gradient in the images is thicker for helium-air cloud than that for hydrogen. This is likely to be related to the difference in front velocity of the clouds which was found to be 0.198 m/s for helium-air cloud compared to 0.181 for the hydrogen-air cloud. The observed gradient differences in the pictures could be also interpreted as the variation in light rays deflection due to the density dissimilarity of the two clouds even if are the same gradients as mentioned in section 2.2.4.

### 2.3.7 Froude number

Froude number is used to describe the pattern of the flows driven by buoyancy. Several studies have explored the relation of inertia forces to buoyancy by Froude number. For instance, Houf et al [23] and Sommersel et al [9, 10]. To verify whether the experimental results accord with previous researches findings, the Froude number was calculated using formula (2.4) for different hydrogen and helium flow rates. Time in the formula defined as the start time recorded by each sensor relative to the first one. Results from the calculations are shown in Figure 2.26.

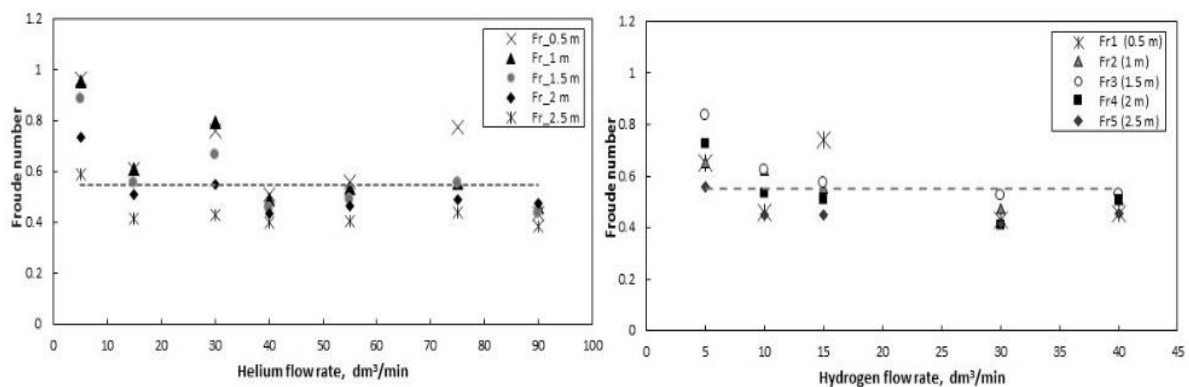


Figure 2.26: Froude numbers for downward releases of helium, (left) and hydrogen, (right) through pipe diameter 4 mm at a flow rate of 40 Ndm<sup>3</sup>/min.

## 2 Hydrogen dispersion

Calculated average Froude number was found to be 0.55 which corresponds dotted lines in Figure 2.26. In order to assess how thoroughly the experimental time data accord with theoretical calculations of Froude number, the time was computed for the obtained average Froude number.

According to Atkinson et al [24], in stably stratified flow condition, Richardson number must exceed 0.25. To evaluate whether the flow in the channel is satisfied the condition  $Ri > 0.25$  or not,  $Ri$  was computed based on Froude number values and average Richardson number found to be 1,35.

Figure 2.27 compares the time calculated theoretically by applying for average Froude number, the solid lines, with experimentally recorded data for helium releases, left and hydrogen, right.

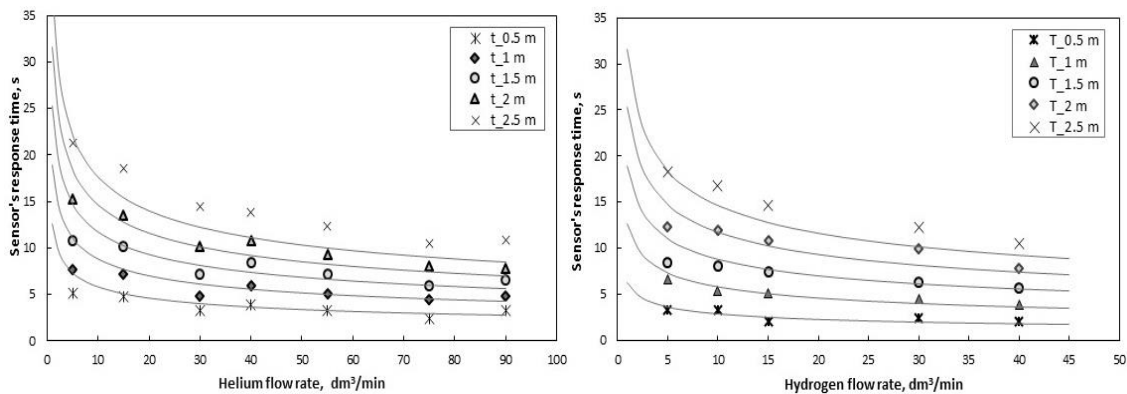


Figure 2.27: Sensor's response time versus flow rate for helium releases (left) and hydrogen (right). Solid lines represent calculated time values for  $Fr = 0.55$ .

There is a difference between obtained Froude number for hydrogen experiments and the previous results reported by Sommersel et al [9, 10] in which the time of ignition determined from the videos recorded by the fast camera and the Froude number has been quantified to be 0.68. A possible explanation for this difference in results might be the variance in time taken by the sensors to measure and record the reading and that for electrode spark and video recording. These results of Froude number so far have only been found from concentration measurements and need to be compared with additional results from ignition experiments under the same conditions. Another possible explanation for this is that the sensor was placed on a hole at the channel ceiling, but the sensor's cap is not reaching the internal ceiling level and small cavity remain there during the measurements as shown in Figure 2.28. The gas accesses the sensing element through diffusion into the cap via a hole in the cap and the cavity might cause disturbances to the cloud front propagation due to the gas vortex movements in the cavity.

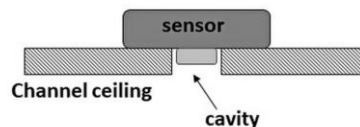


Figure 2.28: Schematic illustration of the positioned concentration sensor in the hole on the channel ceiling

# 3 Hydrogen ignition

## 3.1 Overview of hydrogen ignition

The hydrogen-air mixture is highly flammable over a wide range of compositions (4-75 vol.%) and the minimum energy required for hydrogen gas ignition at normal conditions is 0.02 mJ. So, it can readily be ignited with a high burning velocity. The burning velocity in the hydrogen-air mixture signifies the speed at which combustion wave proceeds in the flammable mixture and it's depending on the temperature, the pressure, and concentration. The burning velocity of stoichiometric hydrogen-air at normal conditions is about 2.55 m/s and 3.2 m/s at 40.1 vol.%. The initiated flame from hydrogen ignition is virtually invisible and emits mainly infrared and ultraviolet radiation [25]. Ignition of a hydrogen-air mixture in confined spaces is frequently related to high risk due to the enhanced effect of confinement on hydrogen accumulation, flame acceleration, and pressure build-up.

Development of premixed hydrogen-air flame in an enclosure is one of the important addressed issues in the field of hydrogen combustion and safety. Hydrogen explosion can cause severe damage to the surroundings. Therefore, the knowledge of the mechanisms underlying the combustion process is fundamental for hydrogen safety and economy.

### 3.1.1 Flame propagation

Several factors could influence the premixed hydrogen-air flame propagation, these include temperature, pressure, geometry, mixture composition, and hydrodynamic instabilities. The flame is unstable because of its vertical movement, created pressure waves and the hydrodynamic instabilities. Depending on the burning velocity, the hydrogen-air flame might generate intensive pressure waves and goes through substantial shape transformations. The growth of combustible products and deformation of the flame lead to an increase in the flame velocity compared to the burning velocity. A large and growing body of literature has investigated hydrogen ignition in addition to the flame propagation behavior and many researchers have provided important information related to the flame velocity, shape, and further expansion. Examples of such studies are found in [26-30].

The originated flame from the ignition of the combustible hydrogen-air mixture is typically propagated with large laminar burning velocity and it's observed to has a spherical shape. This flame has cellular outward form after ignition and turns on to be hemispherical at the wall. This flame is very sensitized to the development of hydrodynamic instabilities. Furthermore, the formation of cellular structure leads to an increase in surface area and subsequently result in flame acceleration [27, 28].

Experimental analysis of hydrogen-air mixture ignition and explosion in a laboratory-scale 1.7 m long, 0.1 m wide and 0.1 m high channel implemented by [31]. Observation of the flame propagation through the channel with the help of high-speed Schlieren videos formed the central focus of the work in which could be clearly seen the flame shape and consequent developments.

### 3 Hydrogen ignition

Figure 3.1 shows an image sequence of flame expansion captured by high-speed Schlieren video at 0.5 m from the channel closed end, after hydrogen release at a flow rate  $10 \text{ Ndm}^3/\text{min}$ . closer inspection of the images signifies the flame evolution, its spherical appearance at 46 ms, (a) after the ignition, then the flame undergoes shape changes while it propagates opposite to the flow direction with the fast growth of the flame surface at 76 ms. (b). The cellular structure can be clearly seen at 100 ms, (c) where the cell surface increases and small new cells appear outward. Further, the number of cells together with the flame surface are increasing rapidly due to the expansion of combustion products at 116 ms, (d).

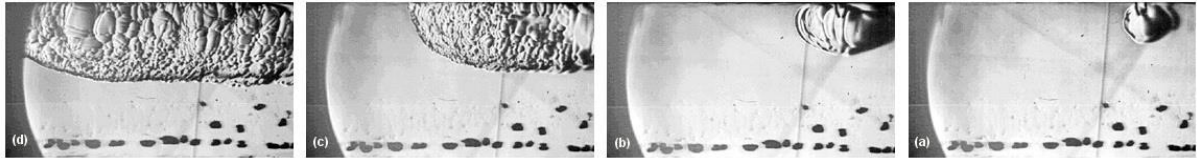


Figure 3.1: Images of the flame propagation after hydrogen release at  $10 \text{ Ndm}^3/\text{min}$  and ignition at 0.5 m from the channel closed end. Images captured by high-speed Schlieren video at (a) 46 ms, (b) 76 ms, (c) 100ms, and (d) 116 ms after the ignition.

## 3.2 Experimental setup

### 3.2.1 The channel and hydrogen supply

combustion experiments of dispersed hydrogen in a 3 m long channel were performed for below-defined scenarios. Materials, dimensions, and volume of the channel are given in section 2.2. The ignition of hydrogen-air combustible cloud was originated on the top of the channel at different locations along the channel and parallel to the release axis. Figure 3.2 illustrates the drawing of the channel setup and appoints ignition and pressure measurement positions and Figure 3.3 displays an image of the channel setup with the pneumatic valve and spark electrodes.

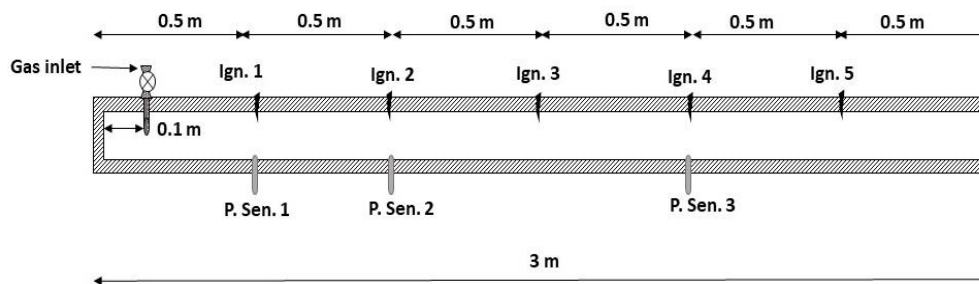


Figure 3.2: schematic drawing of the channel setup with ignition source and pressure's sensors positions



Figure 3.3: Channel setup image viewing the pneumatic valve connected to the release pipe and spark electrodes for ignition

Hydrogen was injected into the channel through a vertical steel pipe diameter 4 mm which was connected to a pneumatic valve, Swagelok to trigger the gas opening. The hydrogen gas was provided from a standard 200 bars cylinder and its volumetric flow rate was regulated by F&P Purgemaster flow meter and Ritter drum-type TG 10/1 was used for calibration of the flow meter before the ignition test was carried out. The pressure at the pneumatic valve was recorded by the KULITE XTM-190 pressure sensor.

### 3.2.2 Ignition and pressure measurements

A high-voltage spark igniter, Siemens ZM 20/10 was used to ignite the flammable hydrogen-air mixture. Electrodes were sparked in a series of short pulses ten times per second and were located on the centerline of the channel's ceiling at different positions lengthways the channel.

### 3 Hydrogen ignition

Figure 3.2 shows the electrodes' five positions on the top of the channel and Figure 3.4 presents the electrodes fixed to the top of the channel.

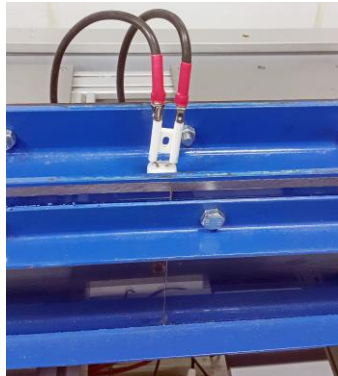


Figure 3.4: electrodes fixed at the channel top.

The pressure in the channel after the ignition and during the flame propagation was measured by Kistler 7001 pressure transducers in three positions at the centerline of the channel's bottom side: 0.5, 1, and 2 m from the channel closed end. The pressure transducers were connected to Kistler 5011B signal amplifiers which were digitally sent the measurements to an oscilloscope as a voltage signal.

#### 3.2.3 Video recording device

Photron SA1.1 high-speed color video camera was operated to record the ignition and flame propagation in the channel. The camera equipped with Nikon, AF NIKKOR 20 mm 1:2.8 D lens and controlled by computer software: Photron FastCam viewer (ver. 3670). To increase the reliability of the recordings with the measurements, the camera was triggered together with the flow opening and pressure measurements devices with the help of Quantum Composer Plus. Recordings were done at a frame rate between 500 and 1000 frs, frames per second, 1024×1024 resolution.

### 3.3 Results and discussion

In this section, results and discussions for hydrogen ignition in the channel were presented. All the experiments were performed for hydrogen injection through a pipe diameter 4 mm and or three flow rates, 15,30 and 40 Ndm<sup>3</sup>/min at five horizontal positions: 0.5, 1, 1.5, 2, 2.5 m from the channel closed end.

#### 3.3.1 Flame propagation

Ignition of combustible hydrogen-air mixture and flame development in the channel were recorded with a high-speed video camera for above-mentioned flow rates. during the experiments, the mixture cloud was ignited by spark at the moment it reached the position of the electrodes. Visualizations for the flame expansion after ignition showed that the thickness and acceleration of the flame were slower for the lower flow rates. In all experiments, it observed that the flame front surface was growing while it propagated towards the injection inlet. Figure 3.5 shows flame propagation development in the channel at a flow rate of 30 Ndm<sup>3</sup>/min and the ignition source was located at 1.0 m from the channel closed end.

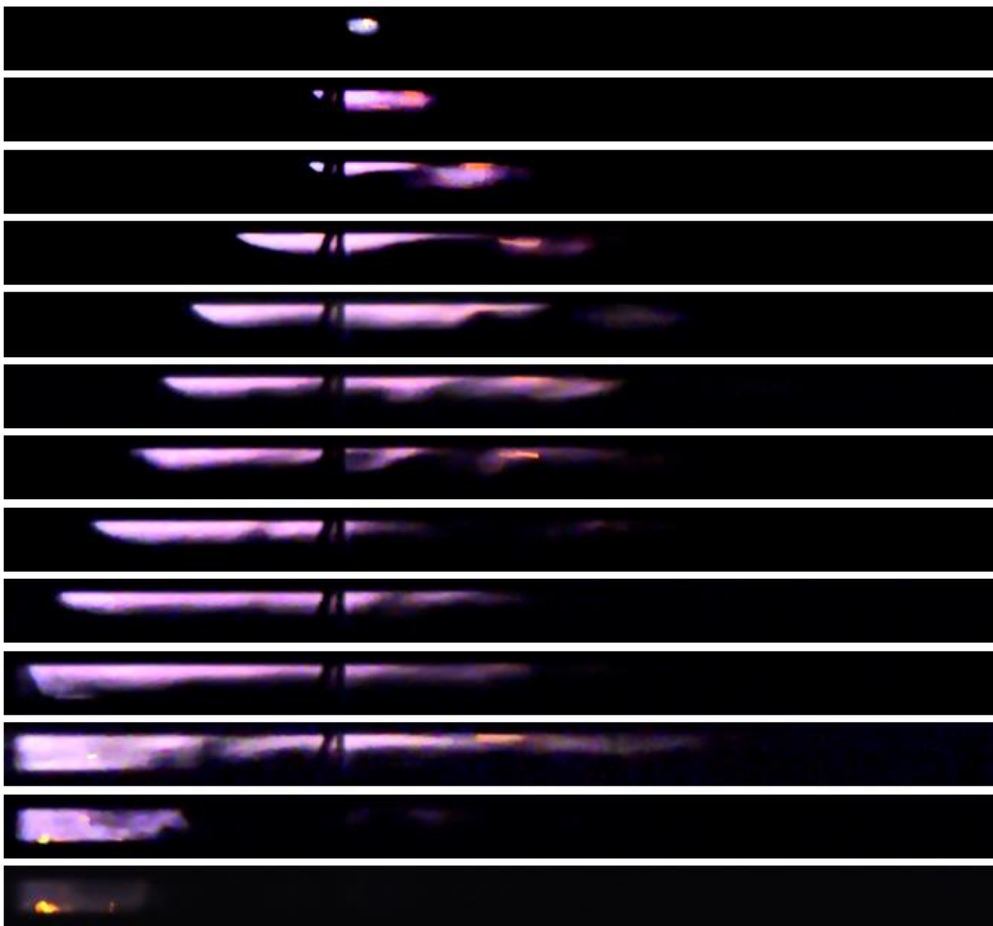


Figure 3.5: Flame propagation in the channel at a flow rate of 30 Ndm<sup>3</sup>/min, at 1 m from channel closed end, and in the duration of 104 s with 8 ms time step.

### 3 Hydrogen ignition

These images are quite revealing in several ways. First, the flame movement from the ignition source began slowly in the direction of the cloud mixture flow and then expanded downstream and upstream. Thereafter, it accelerated with relative higher burning velocity towards the release pipe. Second, it can be seen that the flame occupied just about half of the channel height, a detail which is in agreement with light-fluid intrusion theory. Third, closer inspection of the flame propagation opposite to the flow direction shows that the flame front surface was continuously increasing before it hit the channel closed end. Fourth, the flame shape was controlled by the concentration gradient of the flow ahead of the flame which was characterized by the upper layers with higher hydrogen concentration and the lower layers with excess air at the interface between the cloud and air.

The flame propagation speed has been observed from the movement of the flame front in the channel towards the inlet by high-speed video recordings. Propagation speed was calculated for the above particular test and average speed found to be 13.33 m/s. Figure 3.6 presents the calculated propagation speed against the distance from the channel closed end.

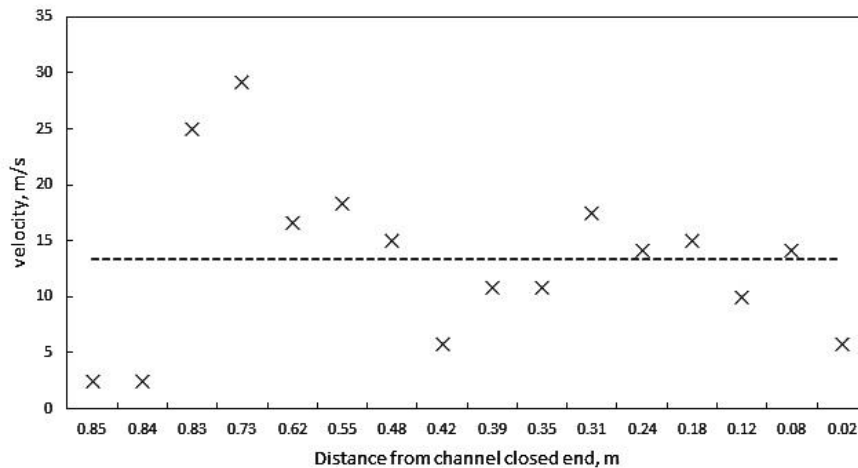


Figure 3.6: Flame propagation speed as a function of distance from the channel closed end at a flow rate of 30 Ndm<sup>3</sup>/min

From the data in Figure 3.6, it can be seen that the flame started with a low constant velocity close to ignition source location, 2.5 m/s, and then propagated with relatively high speed to reach 29.17 m/s for a very short distance. Afterward, it has been decreased and then increased once more and continue varied around 13.33.

Images captured by high-speed video camera display that the propagation speed found to be directly proportional to the flow rate and inversely proportional to the distance between the jet and ignition source. For instance, flame propagation speed for a hydrogen flow rate of 15 Ndm<sup>3</sup>/min and ignition source was placed at 1m from channel closed end, same as the above test, the average speed found to be 11.583 m/s. For a flow rate of 30 Ndm<sup>3</sup>/min and electrodes located at 1 and 2 m from channel closed end, the propagation speeds are 13.33 and 9.981 m/s respectively.



### 3 Hydrogen ignition

Explosion pressures were recorded digitally from three pressure transducers at three positions along the channel: 0.5, 1 and 2 m from the channel closed end. For the above-mentioned test, the overpressures during the combustion process are demonstrated in Figure 3.7. In this figure, the flame shape and position in the channel is displayed at the upper part and the pressure over time graph next down to it. A detailed picture of sinusoidal pressure wave recorded by the three transducers T1, T2 and T3 is given in Figure 3.8.

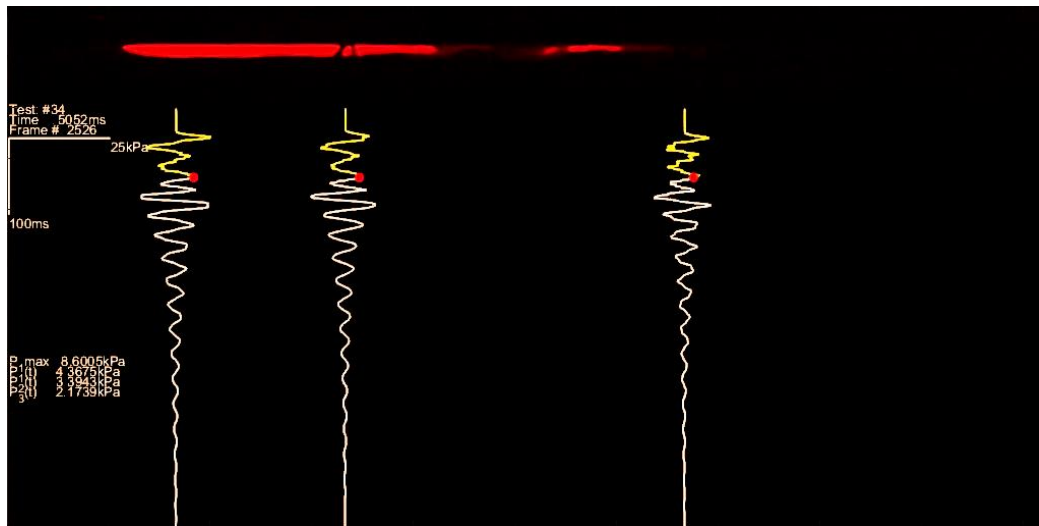


Figure 3.7: Pressure records from 3 transducers at the positions of 0.5, 1 and 2 m from the channel closed end, from left to right, at a flow rate of 30 Ndm<sup>3</sup>/min and ignition source at 1 m.

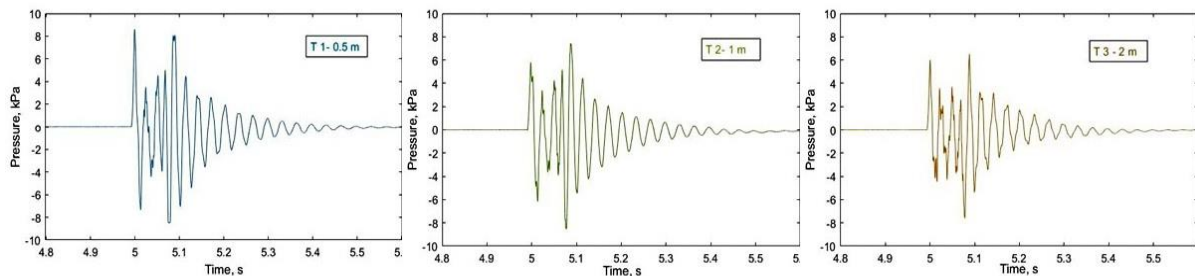


Figure 3.7: Pressure wave records for transducers positioned at 0.5, 1 and 2 m from the channel closed end.

As shown in Figure 3.7, the maximum pressure value recorded was 8.6 kPa from the first transducer at 0.5 m from the channel closed end. Moreover, it displays combustion process conditions where the pressure cursor indicates the middle point between two maximum values 8.6 and 7.997 kPa. This indicates that the overpressure built-up is high close to the ignition source immediately after the ignition and when the flame passes the jet mixing zone and hits the channel closed end. This result may be explained by the fact that the compression effects of the combustion wave lead to an increase in pressure as the flame propagates towards the jet.

### 3.3.2 Comparison of recorded pressures

The overpressure during the ignition and flame development was recorded by pressure transducers which were placed at three positions: 0.5, 1 and 2 m from the channel closed end. Maximum recorded pressures were varied depending on the flow rate, hydrogen release time, and the ignition position. The maximum overpressures recorded during the six explosion tests are presented in table 3.1.

Table 3.1: Recoded pressures during explosion tests at different flow rates and ignition source position from the channel closed end

Flow rate, Ndm <sup>3</sup> /min	15		30		40	
Ignition source position, m	1	2	1	2	1	2
Pressure, kPa	6.389	4.63	8.600	6.984	8.647	8.909

Figure 3.8 shows recorded pressures over time for flow rates (a) 15, (b, c) 30, (d) 40 Ndm<sup>3</sup>/min and ignition source positions (a, b, d) 1, (c) 2 m from the channel closed end. In addition, it shows the flame shape and position at which maximum overpressures have been observed.

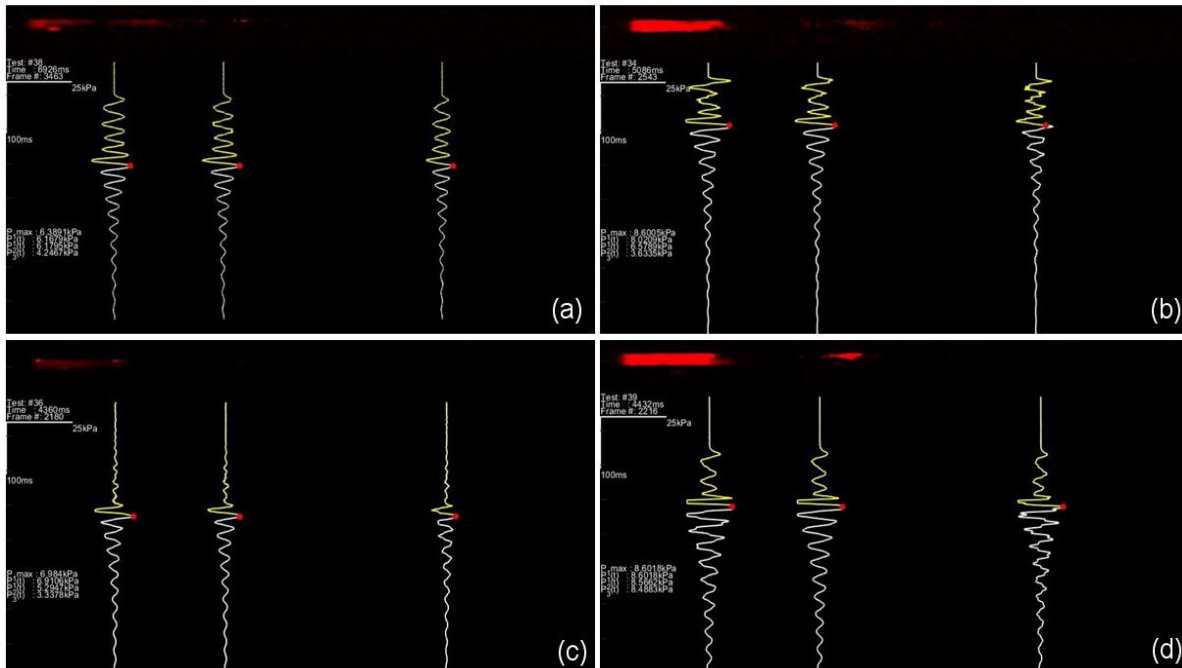


Figure 3.8: Recorded pressures over time where the cursor points the maximum pressure at each transducer for flow rates (a) 15, (b, c) 30, (d) 40 Ndm<sup>3</sup>/min and ignition source positions (a, b, d) 1, (c) 2 m from the channel closed end.

The results from recorded pressures at different flow rates as shown in Table 3.1, indicate that the higher-pressure values were noted at higher flow rates and at the position of the first transducer close to hydrogen inlet. This trend can also be observed in Figure 3.8 which provides a comparison of the shape and flame position at highest recorded pressure position and clearly

### 3 Hydrogen ignition

displays that the pressure peaked when the flame passed through the region around the release pipe and immediately before it hits the channel wall.

The observed highest-pressure peaks at the region between the first transducer and the channel closed end could be attributed to the high hydrogen concentration at the mixing zone around the jet. The flame propagates opposite to the direction of the gradual concentration decay away from the jet due to continuous mixing process with air while the hydrogen-air cloud propagates towards the channel exit.

### 3.3.3 Filled channel scenario

An experiment of a filled channel with hydrogen was performed to investigate the overpressure built-up following hydrogen explosion and trace the flame evolution during the combustion process. Such a scenario might happen under unanticipated leak and accumulation of hydrogen in a tunnel or channel following by ignition and explosion. The channel was filled with hydrogen release at a flow rate of  $40 \text{ Ndm}^3/\text{min}$  through a pipe diameter  $4 \text{ mm}$  and for a duration of  $80 \text{ seconds}$  to have a uniform concentration gradient along the channel. The ignition source was placed at the middle of the channel at  $1.5 \text{ m}$  from the channel closed end. Images captured by a high-speed video camera in the duration of  $72 \text{ ms}$  and  $7 \text{ ms}$  after ignition are illustrated in Figure 3.9.



Figure 3.9: Flame propagation during  $72 \text{ ms}$  and  $7 \text{ ms}$  after the ignition of released hydrogen in the channel at a flow rate of  $40 \text{ Ndm}^3/\text{min}$  and release duration of  $80 \text{ s}$ .

Tracing the flame propagation in Figure 3.9, in the beginning, the flame expanded in two directions upstream and downstream and then accelerated with high velocity towards channel exit and it reached the exit in  $6 \text{ ms}$  with the average propagation speed of  $150 \text{ m/s}$  ( the state at

### 3 Hydrogen ignition

the fourth slice from the top in the above figure). Afterward, the flame expanded gradually in the opposite direction. However, the flame changed its directions during this process and propagated back and forth. The prompt movement of the hydrogen-air mixture towards the exit before the ignition, and the mixture which is kept confined upstream by combustion products after the explosion may have influenced the acceleration towards the exit at the start of the explosion and gradual propagation in opposite direction later.

Figure 3.10 presents the overpressure records over time during the above-mentioned test. The cursor signifies the condition at maximum recorded pressure.

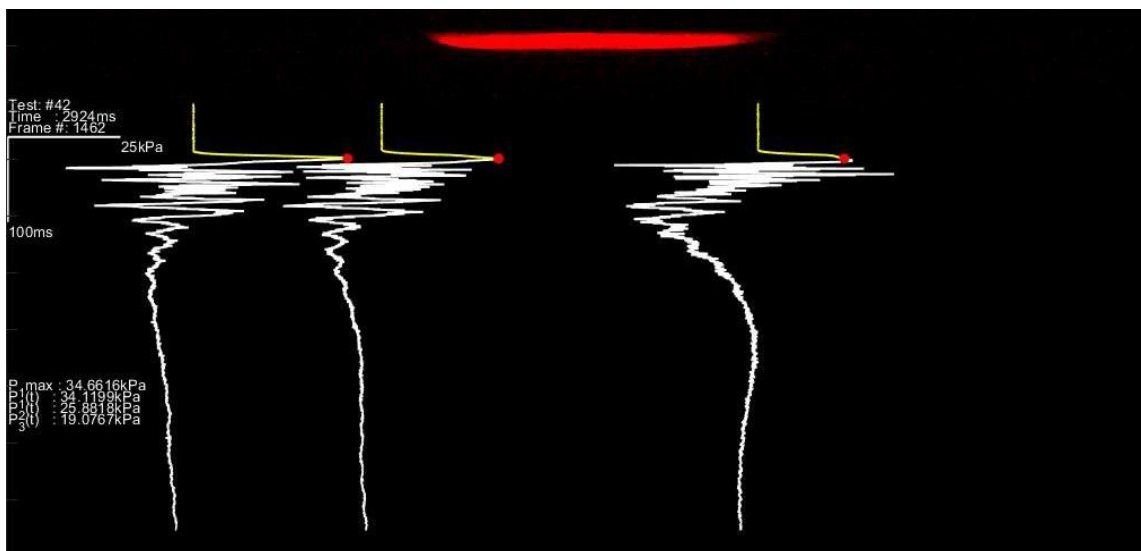


Figure 3.10: the overpressure records over time, the flame shape and position at the highest pressure peak for the filled channel test.

As the channel was filled with a hydrogen-air mixture, it exploded rapidly with relatively high pressures were generated. The highest overpressure, 34.66 kPa, was noted at the first pressure peak from the first transducer directly after the ignition. This condition corresponds to the flame position displayed in Figure 3.10. The second highest pressure was recorded from the third transducer at the third pressure peak and it was 30.16 kPa when the flame accelerated and passed the channel exit. Subsequently, the pressure gradually decreased due to the swift decline in the unburnt hydrogen-air mixture bulk while most of this mixture was burnt.

The variation in the flame front shape can be related to the influence of the pressure waves and the following compression on the flame development in the channel. This leads to a rise in the pressure and consequent amplification of thermal-diffusive instabilities.

Comparing overpressure built-up during combustion of the hydrogen-air mixture in the above-filled channel test with recorded explosion overpressures at the same flow rate, 40 Ndm<sup>3</sup>/min, but different release time: 4.6 and 10.8 s for the ignition source positions 1 and 2 m respectively, the highest pressure peaks are correlated with the position of the flame at the mixing zone around the jet. The pressure-time diagram and the flame position are given in Figure 3.8 (d).

### 3 Hydrogen ignition

Figure 3.11 presents the flame location at maximum pressure peak corresponding the red indicator in the pressure-time graph.

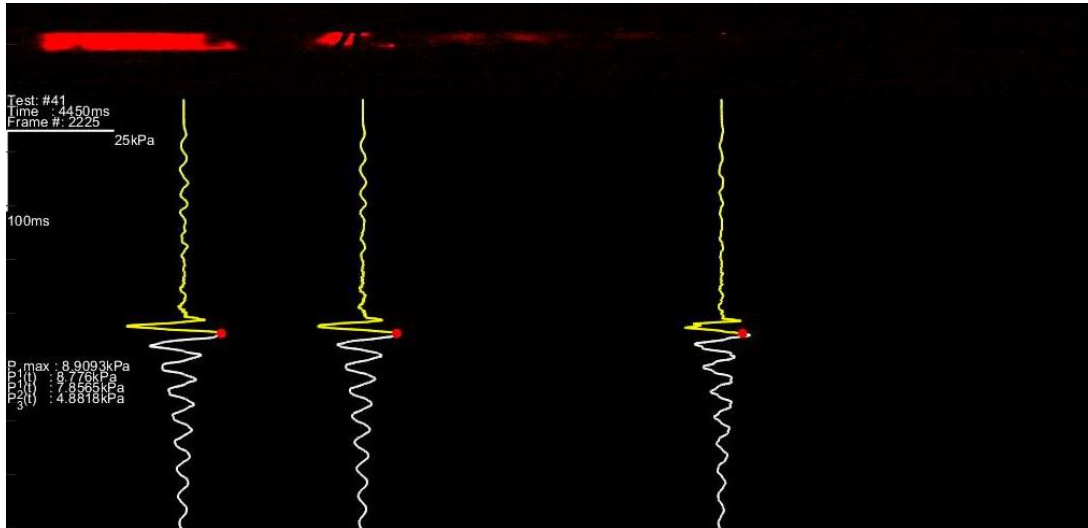


Figure 3.11: the overpressure records over time and the flame shape and position at the highest pressure peak after the ignition at 2 m from channel closed end following hydrogen release at a flow rate of 40 Ndm<sup>3</sup>/min and release time of 10.8 s.

The maximum pressure value for the former was 8.602 kPa and for the latter was 8,909 kPa and this specifies big difference comparing to 34.66 kPa recorded overpressure in the filled channel test.

## 4 Conclusion

The present study is designed to investigate, firstly, the concentration distribution of dispersed hydrogen in partly confined spaces and the parameters influence the concentration in the hydrogen-air cloud, secondly, the flame propagation development and the pressure built-up during the combustion of hydrogen-air mixture in a channel.

A sequence of experiments was carried out on laboratory scale three-meter-long steel channel with transparent polycarbonate sidewalls. A quantitative approach was employed for assessment of helium and hydrogen concentration distribution along the channel by using WIFI read out concentration sensors. Concentrations were measured at various horizontal and vertical positions for releases at different flow rates, through different nozzle sizes and different injection directions. Furthermore, concentrations were measured along an inclined channel by positive and negative ten degrees. Flow visualization technique was applied with the assistance of Background-Oriented Schlieren and Shadowgraph along with high-speed video camera to record, image the concentration gradients of the mixing process next to the release point and the cloud propagation at the middle of the channel.

The results from these experiments indicate that the mixing of helium and hydrogen with air occur rapidly at higher flow rates, smaller nozzle sizes, and downward release direction. Moreover, these experiments confirmed that jet momentum- induced mixing to happen close to the release point and wave buoyancy-induced, away from it. Higher concentrations recorded in the channel with a negative inclination channel with negative inclination has higher recorded concentrations due to the lower helium-air mixing rate.

Dispersion of helium and hydrogen in the channel characterized by the formation of inhomogeneous and stratified mixture cloud. The relevance of mutual intrusion theory is clearly supported by flow imaging results which indicate that the helium-, hydrogen-air cloud performs as a gravity current. The Froude number was calculated based on the start reading-out from the concentration sensors and the result is not in complete accord with the results from previous studies.

A laboratory-scale experimental arrangement was utilized to run hydrogen-air cloud explosion tests. A 3 m long channel was equipped with electrodes as an ignition source, pressure transducers, and high-speed video camera to record the ignition and flame propagation in the channel. Data from video recordings were used to analyze the flame propagation velocity, shape, and position to compare with recorded overpressure data.

Results obtained from experiments with a release time between 4.6 and 11.4 s show that maximum generated overpressures were between 4 and 9 kPa. However, the highest pressure peak for explosion test in a filled channel with hydrogen mixture cloud in the duration of 80 s was 34.66 kPa.

In explosions occur after short release time in a channel, the maximum pressure generated when the flame passes through the mixing zone around the jet, while for long time release, it produced directly after the ignition. the test with a filled channel could be a real scenario of the unintended leak, dispersion, and ignition of hydrogen in a tunnel or channel, therefore, the results from the filled channel test can be useful to obtain valuable information relating to fire development and characteristics based on scaling technique.

#### 4 Conclusion

Overall, the analysis was done by this study have a number of practical applications in the field of hydrogen safety. In addition, it contributes to the existing knowledge of hydrogen dispersion and explosion in confined spaces by providing practical data for further analyses.

This project has investigated helium concentration distribution in an inclined channel. However, further studies are needed to examine the ignition and subsequent flame propagation of the hydrogen-air mixture in an inclined channel. Regarding not complete agreement of calculated Froude number with the previous research, further investigations by different methods should be done to re-evaluate the finding.



# References

- [1] N. Armaroli and V. Balzani, "The Hydrogen Issue," *ChemSusChem*, vol. 4, no. 1, pp. 21-36, 2011/01/17 2011.
- [2] E. Miller, "Hydrogen Production Program-Overview," Annual merit review and peer evaluation, Washington D.C 2017.
- [3] L. Cadwallader and J. Herring, *Safety Issues with Hydrogen as a Vehicle Fuel*. Lockheed Martin Idaho Technologies Company, 1999.
- [4] S. Gupta, J. Brinster, E. Studer, and I. Tkatschenko, *Hydrogen related risks within a private garage: Concentration measurements in a realistic full scale experimental facility*. 2009, pp. 5902-5911.
- [5] K. Brady, C.-J. Sung, and J. T'ien, *Dispersion and catalytic ignition of hydrogen leaks within enclosed spaces*. 2012, pp. 10405–10415.
- [6] K. Takeno, K. Okabayashi, A. Kouchi, T. Nonaka, K. Hashiguchi, and K. Chitose, *Dispersion and explosion field tests for 40 MPa pressurized hydrogen*. 2007, pp. 2144-2153.
- [7] M. De Stefano, X. Rocourt, I. Sochet, and N. Daudey, "Hydrogen dispersion in a closed environment," *International Journal of Hydrogen Energy*, vol. 44, no. 17, pp. 9031-9040, 2019/04/02/ 2019.
- [8] J. M. Lacome, D. Jamois, L. Perrette, and C. H. Proust, "Large-scale hydrogen release in an isothermal confined area," *International Journal of Hydrogen Energy*, vol. 36, no. 3, pp. 2302-2312, 2011/02/01/ 2011.
- [9] O. K. Sommersel, D. Bjerketvedt, K. Vaagsaether, and T. K. Fannelop, "Experiments with release and ignition of hydrogen gas in a 3 m long channel," *International Journal of Hydrogen Energy*, vol. 34, no. 14, pp. 5869-74, 2009.
- [10] O. K. Sommersel, *Hydrogen leaks in partially confined spaces - dispersion and explosions*. Porsgrunn: University College of Southeast Norway, 2017.
- [11] J. He, E. Kokgil, L. Wang, and H. D. Ng, "Assessment of similarity relations using helium for prediction of hydrogen dispersion and safety in an enclosure," *International Journal of Hydrogen Energy*, vol. 41, no. 34, pp. 15388-15398, 2016/09/14/ 2016.
- [12] W. M. Pitts, J. C. Yang, and M. G. Fernandez, "Helium dispersion following release in a 1/4-scale two-car residential garage," *International Journal of Hydrogen Energy*, vol. 37, no. 6, pp. 5286-5298, 2012/03/01/ 2012.
- [13] M. R. Swain and J. Shriber, *Comparison of Hydrogen, Natural Gas, Liquefied Petroleum Gas, and Gasoline Leakage in a Residential Garage*. 1998.
- [14] G. bernard-michel and D. Houssin-Agbomson, "Comparison of helium and hydrogen releases in 1 m<sup>3</sup> and 2 m<sup>3</sup> two vents enclosures: Concentration measurements at different flow rates and for two diameters of injection nozzle," *International Journal of Hydrogen Energy*, vol. 42, 2016.
- [15] V. Molkov, *Fundamentals of Hydrogen Safety Engineering*. HySafer center - university of Ulster, 2012.

- [16] HySafe. (2009). *Accidental Phenomena and Consequences -Section 1.01-Release of Hydrogen*. Available: [https://www.hysafe.org/download/1003/BRHS\\_Chap3\\_release\\_version%200\\_9\\_0.pdf](https://www.hysafe.org/download/1003/BRHS_Chap3_release_version%200_9_0.pdf)
- [17] J. E. Simpson, *Gravity Currents: In the Environment and the Laboratory*. Cambridge University Press, 1999.
- [18] H. Ingason, Y. Li, and A. Lönnemark, *Tunnel Fire Dynamics*. New York: Springer science media New York, 2015.
- [19] T. K. Fannelöp, *Fluid Mechanics for Industrial Safety and Environmental Protection (Industrial Safety Series )*. Elsevier Science, 1994.
- [20] A. Mazumdar, "Principles and Techniques of the Schlieren Systems.," Columbia University New York, 2013.
- [21] G. Settles and M. Hargather, *A review of recent developments in schlieren and shadowgraph techniques*. 2017.
- [22] E. Rathakrishnan, *Instrumentation, Measurements, and Experiments in Fluids*. CRC Press, 2016.
- [23] W. G. Houf and R. Schefer, *Analytical and experimental investigation of small-scale unintended releases of hydrogen*. 2008, pp. 1435-1444.
- [24] G. Atkinson, E. Cowpe, J. Halliday, and D. Painter, "A review of very large vapour cloud explosions: Cloud formation and explosion severity," *Journal of Loss Prevention in the Process Industries*, vol. 48, pp. 367-375, 2017/07/01/ 2017.
- [25] L. M. Gandia, G. Arzamedi, and P. M. Dieguez, "Hydrogen hazards and risks analysis through CFD simulations," in *Renewable Hydrogen Technologies: Production, Purification, Storage, Applications and Safety* Spain: Newnes, 2013.
- [26] J. Beeckmann *et al.*, "Propagation speed and stability of spherically expanding hydrogen/air flames: Experimental study and asymptotics," *Proceedings of the Combustion Institute*, vol. 36, no. 1, pp. 1531-1538, 2017/01/01/ 2017.
- [27] K. Rai, D. Bjerketvedt, and O. K. Sommersel, *Experimental Study of the Initial Flame Propagation of Premixed H<sub>2</sub>-air Explosion in a Channel*. 2009.
- [28] C. R. L. Bauwens, J. M. Bergthorson, and S. B. Dorofeev, "Experimental investigation of spherical-flame acceleration in lean hydrogen-air mixtures," *International Journal of Hydrogen Energy*, vol. 42, no. 11, pp. 7691-7697, 2017/03/16/ 2017.
- [29] R. Addabbo, J. K. Bechtold, and M. Matalon, "Wrinkling of spherically expanding flames," *Proceedings of the Combustion Institute*, vol. 29, no. 2, pp. 1527-1535, 2002/01/01/ 2002.
- [30] H. Xiao, Q. Duan, and J. Sun, *Premixed flame propagation in hydrogen explosions*. 2017.
- [31] K. Rai and D. Bjerketvedt, "Experimental results from flame propagation in a channel," ed. Porsgrunn, Norway: Private communication-University of South-Eastern Norway, 2019.

# Appendices

Appendix A: Master's Thesis Description

Appendix B: Safety Procedures and Regulation in The Machinery Hall

Appendix C: Risk evaluation and safety directions of laboratory experiments

Appendix D: Job Safety Analysis

Appendix E: Concentration Measurement Results

Appendix F: Hydrogen Explosion Tests Results

Appendix G: Instrumentation

Appendix H: "Experimental study of light gas dispersion in a channel"

Draft paper was written to ICHS 2019

## Appendix A: Master's Thesis Task Description



Faculty of Technology, Natural Sciences and Maritime Sciences, Campus Porsgrunn

### FMH606 Master's Thesis

**Title:** Dispersion of hydrogen in confined spaces

**USN supervisor:** Prof. Dag Bjerketvedt

**External partner:** MoZEEs and HyTunnel and CS

**Task background:**

In the case of an accidental jet release of hydrogen in a partially confined area, walls, ceilings and other objects will limit the dispersion. The objective of this thesis is to study the momentum-controlled jet and the buoyancy-controlled wave in partly confined spaces. The goal is to identify which parameters influences the hydrogen concentration in the cloud and the height of the combustible cloud when a hydrogen jet hits a ceiling. This thesis is part of i) RA3 activity in *MoZZES* ([www.mozees.no](http://www.mozees.no)) and ii) the EU Horizon 2020 *HyTunnel and CS (Confined Spaces)* project .

**Task description:**

- Literature review on hydrogen jet releases in confined areas with focus on jet dispersion, gravity currents and flame propagation in inhomogeneous gas clouds.
- Arrange a test rig for dispersion and explosion testing in the lab. Diagnostics includes gas and pressure sensors and high-speed video.
- Perform experiments the rig
- Optional : CFD simulation with OpenFOAM

**Student category:** EET, EPE, IIA or PT students

**Practical arrangements:**

**Supervision:**

15-20 hours of supervision

**Signatures:**

Supervisor (date and signature):

1/2 - 2017 Dag Bjerketvedt

Student (date and signature):

1/2 - 2019

Student :

Osama Kabbashi Mohammed Ibrahim

**Address:** Kjølnes ring 56, NO-3918 Porsgrunn, Norway. **Phone:** 35 57 50 00. **Fax:** 35 55 75 47.

## Appendix B: Laboratory Safety Procedures



Porsgrunn, January 17<sup>th</sup>, 2019

### Review of safety procedures and regulations in the Machinery Hall: a checklist

The checklist applies to all staff and students who will be carrying out projects or laboratory practice in the machinery hall and for external visitors, including hired workers, who are going to do work in the machinery hall. The person responsible for an apparatus or the safety officer must go through the check list.

The following points must be gone through<sup>1</sup>:

- Say if there is a safety officer present in the Machinery Hall, and who this is<sup>2</sup>
- Show where the safety equipment is located
  - First aid kit (go through the contents if needed)
  - Fire hose
  - Safety spectacles (must be put back after use)
  - Hearing protection
  - Helmet with hearing protection
  - Stretcher
  - Fire blanket
  - Fire extinguishers (explain how they work, if necessary)
  - Emergency shower
  - Fire alarms
  - Bottles of emergency eyewash (see map)
  - Laser safety goggles
- Show the location of the fire exits
- Show the whereabouts of the material safety data sheets
- Point out that it is necessary to tidy up one's work place every day
- Point out that gas bottles shall be properly secured when they are placed in the Machinery Hall.
- In the case of hot work<sup>3</sup>: ask for permission from the safety officer before the work commences. Inform Statsbygg (deactivate fire alarm) Cover all flammable materials.
- Give information about any special elements of risk at the various apparatus.
  - Laser (CVL and Firefly)
  - Pressurized and flammable gas

I declare that I have participated in a review of the safety procedures and regulations in the Machinery Hall.

Student number: 213074 Name: M. Ibrahim Osama

Signature: 

Class: ..... Date: 17.01.2019

<sup>1</sup> Can be omitted if it can be documented that this part has already been reviewed during the present college term

<sup>2</sup> The name and telephone number is on the room card

<sup>3</sup> E.g. welding or the use of a cutting wheel

## Appendix C

### Risk Evaluation and Safety Directions of Laboratory Experiments

Faculty of Technology, Natural Sciences and Maritime Sciences, Campus Porsgrunn

#### 1. FMH606 Master's Thesis

**Thesis title:** Hydrogen Dispersion in Confined Spaces

**USN supervisor:** Prof. Dag Bjerketvedt

**Student:** Osama Kabbashi M.Ibrahim

#### 2. Introduction

For the safe handling of hydrogen, it is important to know its properties and the necessary safety measures. Hydrogen is a highly flammable gas. If not handled and stored properly, Hydrogen gas can pose a serious threat to the health and safety of laboratory personnel, emergency respondents and, the equipment. Hydrogen gas forms explosive mixtures with air when H<sub>2</sub> concentration between 4 and 74% and the mixture spontaneously explodes by spark, heat or sunlight. Auto-ignition temperature of Hydrogen is 500 °C. Hydrogen reacts with every oxidizing element and dissolves in many metals.

Physical & Chemical Properties:

Class:	highly Flammable gas
Color:	Colorless
Phase:	Gas
Density:	0.08988 g/L (0 °C, 101.325 kPa)
Melting point:	-259.14 °C
Boiling point:	-252.87 °C
Molar Heat Capacity:	28.836 J·mol <sup>-1</sup> ·K <sup>-1</sup>

The hazards of hydrogen mixed with air include potential explosions and fires. To be asphyxiation when it's pure. This guideline helps to understand how to properly store and handle hydrogen.

#### 3. Potential Hazards

Hydrogen gas is highly flammable and will burn in air at a very wide range of concentrations between 4% and 75% by volume.

Storage Requirements: hydrogen cannot be stored in the same fire compartment as oxidizing substances.

An acceptable Safety level can be achieved while handling hydrogen gas by the following

instructions:

- a) Ventilation: Prevent accumulations of leaked hydrogen by ensuring adequate ventilation which reduces the risk of leaked hydrogen gas building up to flammable concentrations in the laboratory. Since hydrogen is such a light molecule, it can accumulate near the ceiling unless forced ventilation systems are used in which air extraction occurs at the highest point in the room.
- b) Eliminate likely ignition sources, and suspect unknown ignition sources.
- c) verify the system has been purged to less than 1 percent when performing system maintenance on a hydrogen system. Inert gases can be used for purging.
- d) Excess flow valves or flow restricts should be used to control maximum hydrogen flow
- e) appropriate PPE (e.g., safety glasses, laboratory coats, gloves, face shields) based on specific hazards.
- f) Protection shields/ boards should be used when experiments with ignition and explosion are implemented

#### **4. Cylinder handling**

- Compressed gas cylinders should be double chained or strapped to a stable structure.
- Never roll, drop or lift cylinders by their protective caps.
- Cylinders in the laboratory should be equipped with a pressure regulator designed for hydrogen and marked for its maximum cylinder pressure. Regulators should be equipped with two gauges, installed to show both the cylinder pressure and the outlet pressure.
- Remove the regulator and place the safety cap on, when the cylinder is not in constant use.

#### **5. Types of Emergencies**

- The principal danger from a leak is the potential of burns and fires.
- When a leak occurs, the area shall be completely roped off and caution signs shall be posted.
- Leaks can occur near the valve/regulator/tubing/tubing bends or joints or a pumping system.
- Catastrophic explosions can occur.
- High-pressure gas leaks can occur.

#### **6. Measures should be taken when**

##### **A) Gas Leaks from Cylinders:**

- If a cylinder safety device leaks, personnel shall not attempt to correct the leak by tightening the safety device cap while the cylinder is under pressure.
- The contents of the cylinder shall be emptied in a safe location.
- The cap shall be removed to examine the condition of the threads, correct the damage, pressurize and leak test.
- Hydrogen gas cylinders must be secured in an upright position to avoid being knocked

over.

**B) If a leak is detected:**

- Evacuate the immediate area of all personnel
- Immediately shut off the hydrogen source
- To detect a small local hydrogen fire (the flame is nearly invisible), use a piece of tissue paper on a stick, the paper will readily ignite upon contact with the flame.

**C) uncontrollable leaks**

- The supply source shall be shut-off immediately if possible
- The area shall be evacuated
- Contact laboratory safety officer immediately.

**D) In case of fire**

- Refer to USN's fire instructions

**Porsgrunn**

**Date:** 17.01.2019

**Signature:** *Osamak*

**References:**

[1] (2018). *Hydrogen Laboratory Safety* Available:  
<https://h2tools.org/bestpractices/laboratory-safety>

[2] H. a. S. I. f. t. B. C. Environment. (2013). *Fact Sheet: Hydrogen Safety*. Available:  
<https://www.ehs.berkeley.edu/sites/default/files/lines-of-services/workplace-safety/80hydrogen.pdf>



## Appendix D: Job Safety Analysis

<b>USN (University of South-Eastern Norway)</b>	
Job Safety Analysis (JSA)	Case and doc. no 2019/1
	Page: 1 of 2
Prepared by: Osama Kabbashi M. Ibrahim	Date: 17.01.2019 Edition: 1

### Job task to which this Job Safety Analysis applies:

Examination of helium and hydrogen dispersion in confined spaces

**Responsible employer:** Prof. Dag Bjerketvedt

**Time of performance of the work:** 07.01.2019 – 15.05.2019

**Persons involved in the performance of the work:** 1

### Description of the work:

1. Concentration measurements of helium and hydrogen released in a channel.
2. Pressure measurements during hydrogen ignition and explosion.

**Training required:** Yes

### PPE and other protective equipment to be used:

Gloves, nose mask, safety goggles, and a laboratory coat.

**Analysis:** (List the sub-tasks and assess hazards, e.g. heavy lifting, repetitive movements, eye injury, cuts, falls, crush injuries, allergies. List preventive measures that have been or must be implemented. Preventive measures must be completed before the start of work).

<b>Sub-tasks</b>	<b>Hazards</b>	<b>Preventive measures</b>	<b>Deadline</b>	<b>Status</b>
Run the explosion tests with hydrogen	Thermal burns, cuts, hearing impairment, and eye injury related to fires and explosion.	Use of fire-proof shields, and leather gloves. Use of earplugs or headphones Wear goggles, laboratory coat,	15.05.2019	In progress
Change the position of the electrodes in ignition tests	Electrical shock	Use insulation equipment and gloves	15.05.2019	In progress
Installation of experiments setup	Hand cuts and heavy lifting	Wear protective gloves and adequate support is provided	15.05.2019	In progress

### Participants in the analysis and signatures

<b>Role</b>	<b>Name</b>	<b>Date/signature</b>
Supervisor	Prof. Dag Bjerketvedt	
Participant /student	Osama M. Ibrahim	17.01.2019 <i>Osama</i>

## Appendix E: Results from hydrogen dispersion experiments

### 1- Vertical concentration distribution

In sections 2.3.1 – 2.3.3, helium vertical concentration distribution was given at the horizontal location 2.5 m from the channel closed end. However, vertical measurements were also performed simultaneously at the channel exit. It is interesting to compare these results with those which were done at 2.5 m, in the mentioned sections. Figure 1 presents helium output concentration as the function of time at cited vertical locations for downward release through 1 mm nozzle and at the channel exit, 3 m from the channel closed end.

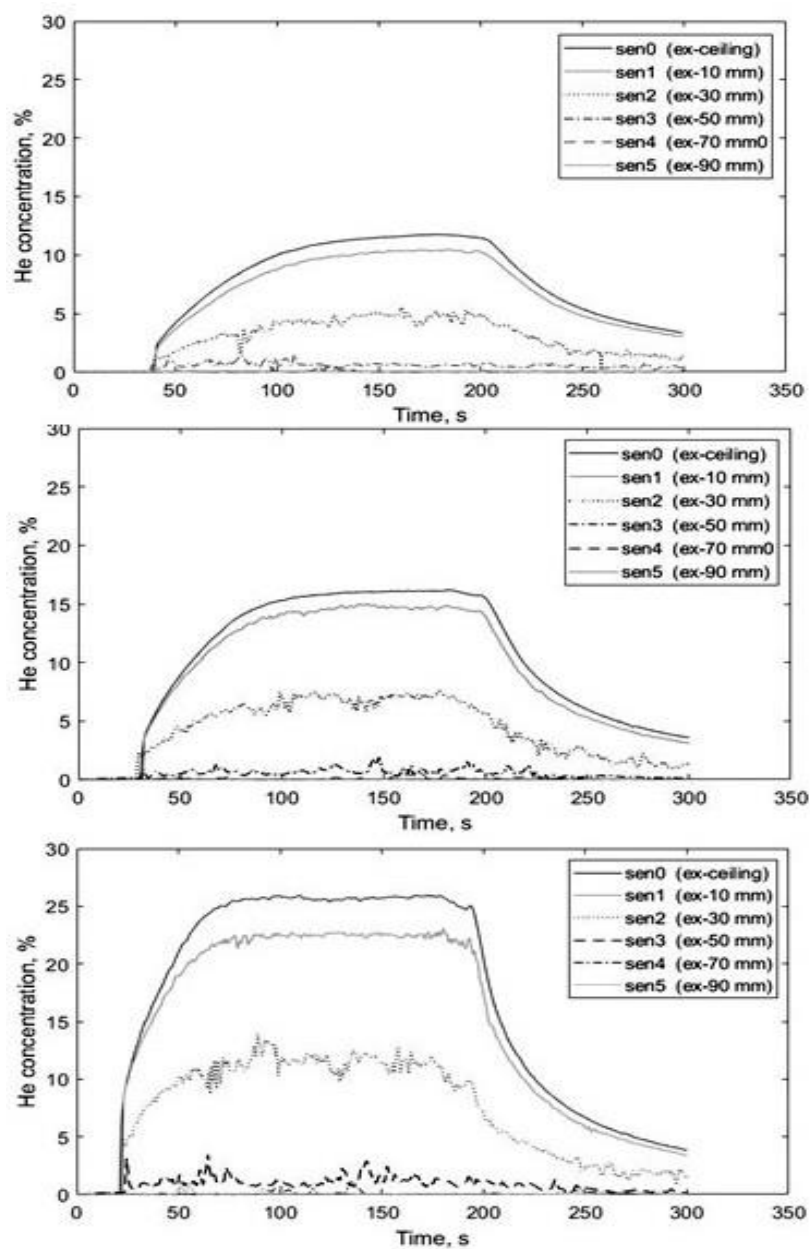


Figure 1: Distribution of helium concentration vertically at the channel exit over time for downward release through 1mm nozzle size and at flow rates: (top) 5, (middle) 15 and (bottom) 40 Ndm<sup>3</sup>/min.

**2- Helium release through 0.5 mm nozzle size**

Figure 2 illustrates measurements of concentration at six locations along the channel for helium upward release at 5 and 15 Ndm<sup>3</sup>/min, through the nozzle diameter 0.5 mm.

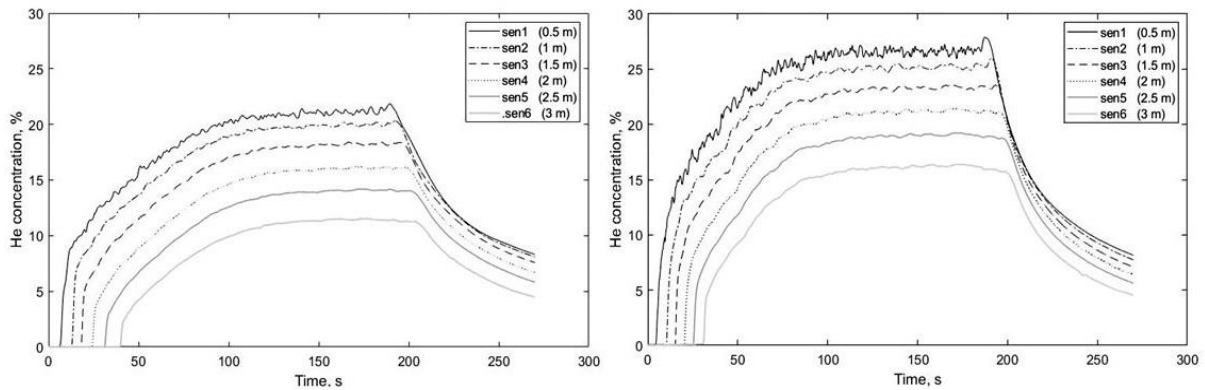


Figure 2: Helium concentration as the function of time for upward release through 0.5 mm nozzle size and at flow rates: (left) 5 and (right) 15 Ndm<sup>3</sup>/min.

**3- The pressure at the inlet of the pneumatic valve**

The pressure was measured by Kulite pressure sensor at the inlet of the pneumatic valve in experiments of helium and hydrogen comparison, and hydrogen explosion. Figure 3 shows the pressure profile for 4 minutes of hydrogen release at a flow rate of 40 Ndm<sup>3</sup>/min through a pipe diameter 4 mm, and Figure 4 presents the pressure profile for hydrogen release at flow rates 15 and 40 Ndm<sup>3</sup>/min and through a nozzle size of 0.5 mm.

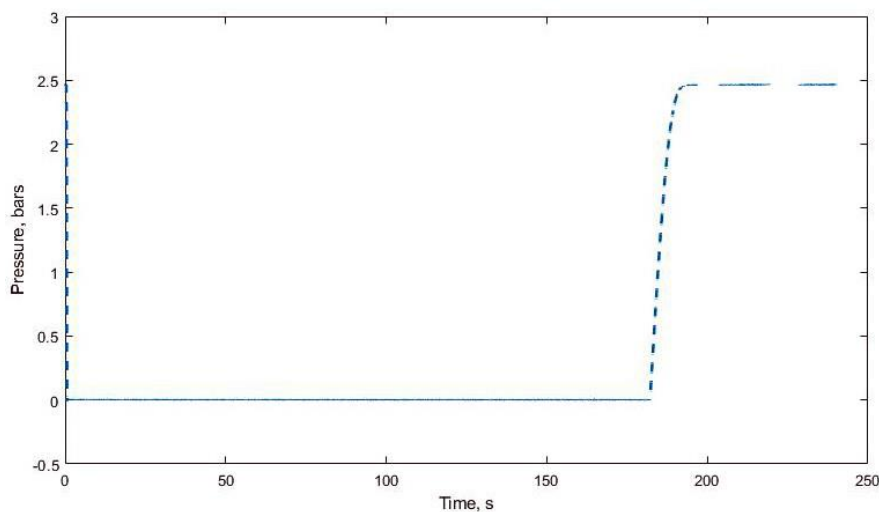


Figure 3: Recorded pressure over time for hydrogen downward release at 40 Ndm<sup>3</sup>/min through 4 mm diameter pipe

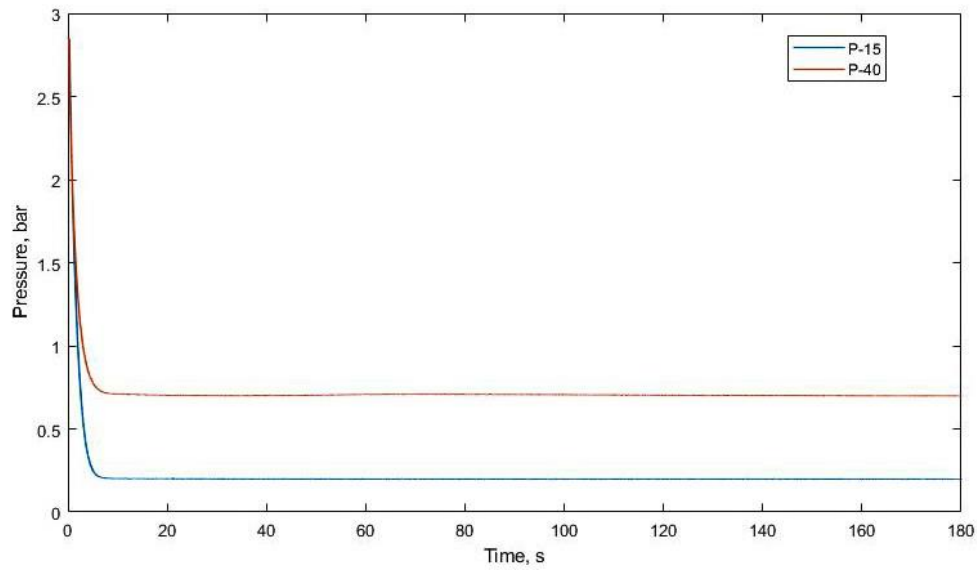


Figure 4: The pressure as a function of time for hydrogen downward release at 15 and 40 Ndm<sup>3</sup>/min through a nozzle diameter 0.5 mm.

**4- Cloud shape at different flow rates**

Figure 5 compares the helium-air mixture cloud in the middle of the channel at the helium downward release rate of 50 and 10 Ndm<sup>3</sup>/min from a pipe diameter of 4 mm.

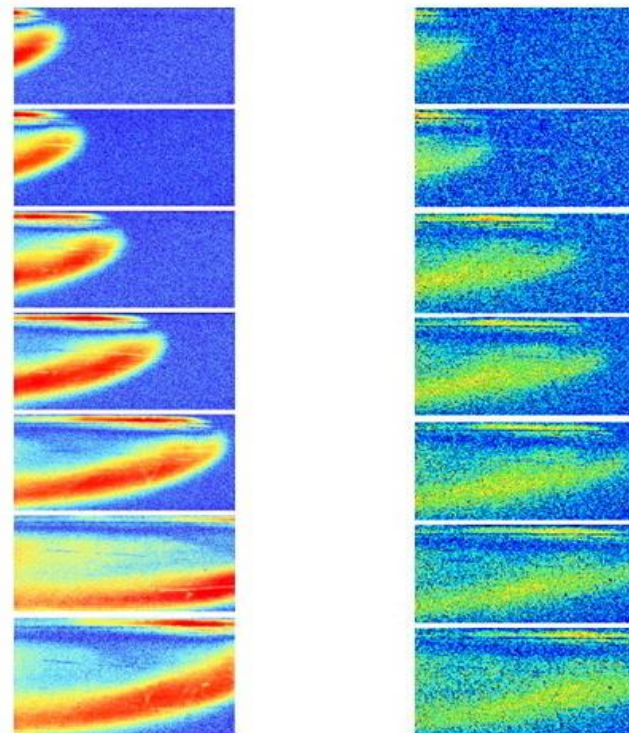


Figure 5: Images of the cloud captured at 1.5 m from the channel closed end for helium downward release at flow rates 50, left and 10 Ndm<sup>3</sup>/min, right, and through a pipe diameter 4 mm.

## Appendix E: Results from hydrogen explosion experiments

### 1- Flame propagation

The flame propagation in the channel following the ignition of the hydrogen cloud for downward hydrogen release at a flow rate of 40 Ndm<sup>3</sup>/min and through a pipe diameter 4 mm are illustrated in Figures 6 and 7.

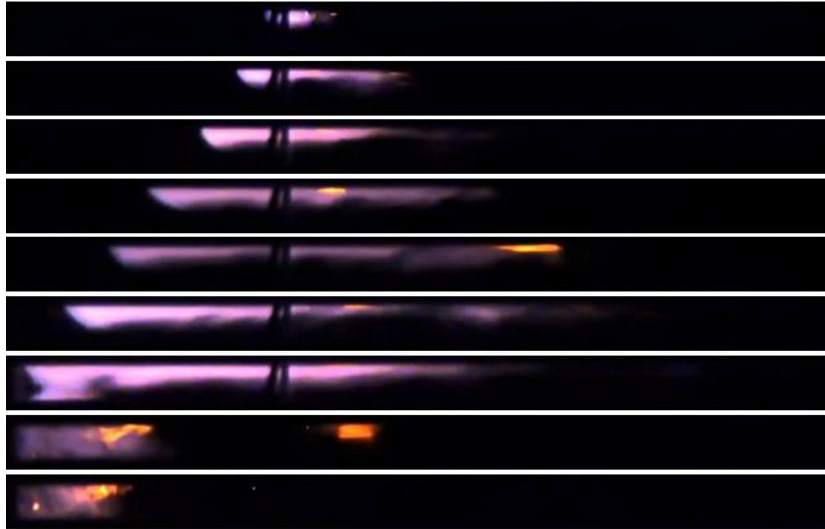


Figure 6: Flame propagation in the channel after the ignition of the hydrogen-air cloud. The ignition source was placed 1 m from the channel closed end.

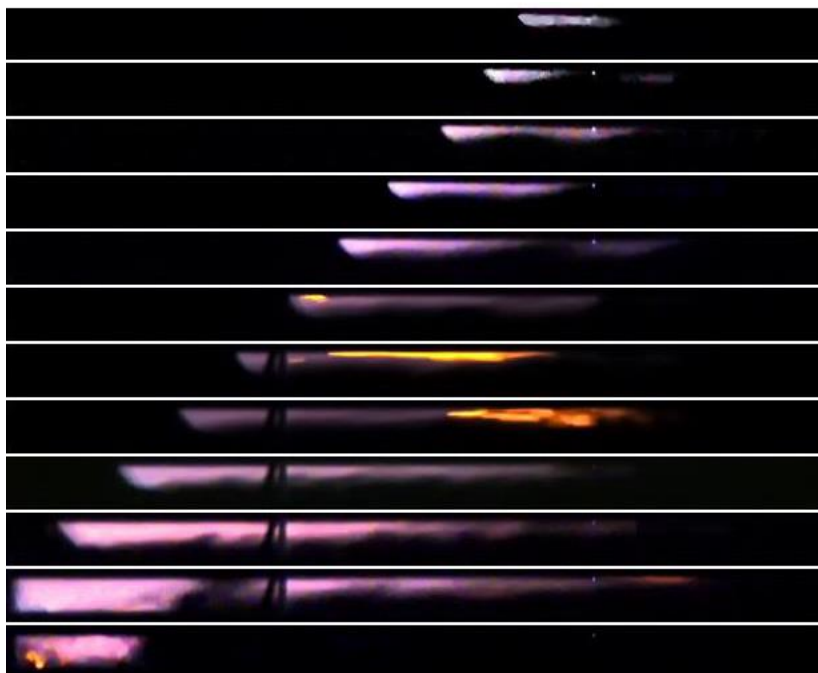
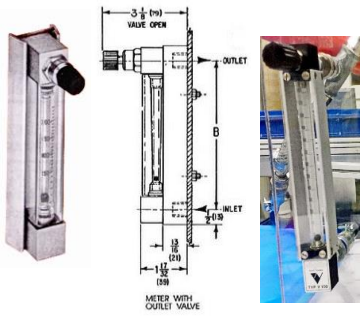




Figure 7: Flame propagation in the channel after the ignition of the hydrogen-air cloud. The ignition source was placed 2 m from the channel closed end.



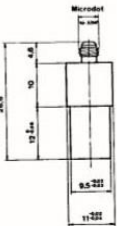


## Appendix G: Instrumentation

The tables below give a brief description of all equipment used to perform the experimental work for this study. There is concise information about the application, materials, images, and technical characteristics. This appendix contains also references to where this information was picked up.


### (a) Gas flow equipment

 <p>The image shows a vertical glass tube flow meter with a stainless steel body. On the left is a photograph of the physical device. On the right is a technical cross-section diagram. The diagram labels the 'VALVE OPEN' position at the top, the 'OUTLET' at the top of the tube, and the 'INLET' at the bottom. Dimensions are provided: 3 1/2 (90) for the top section, 1 1/2 (38) for the bottom section, and 'B' for the main tube length. A note at the bottom reads 'METER WITH OUTLET VALVE'.</p>	<p>The ABB Automation Purgemaster flow meter is a low capacity, glass tube type, variable area meter used to measure and visually indicate the flow rates of gases and it is ideal for such applications as the purging of control lines and instrument enclosures. High Strength Stainless Steel Body – Rigid construction to maintain tube alignment and resistance to pipe strain. The optional control valve provides a smooth fine degree of adjustment. Materials: glass tube and stainless-steel body [1]</p>
 <p>The image shows a circular, stainless-steel gas meter with a white face and black markings. The brand name 'Ritter' is visible on the dial. It has two ports on top and is mounted on four small feet.</p>	<p>RITTER TG 0/1 gas meters were used for calibration of Purgemaster flow meter. RITTER TG 0/1 works on the principle of positive displacement. It is manufactured from stainless-steel for Maximum constant use temperature 40 °C and performance data: Minimum flow: 20 L/h, Standard flow: 1000 L/h, Measurement accuracy at standard flow 0.2 %. Maximum gas inlet pressure: 500 bar [2].</p>
 <p>The image shows a Swagelok pneumatic actuator, which is a rectangular metal device with a black knob on top and various ports. A second image shows the actuator installed on a blue pipe, demonstrating its use in controlling a ball valve.</p>	<p>Swagelok Pneumatic Actuator, ball valve with 2-way (straight and angle) flow paths, 90° actuation and Spring-return. Output torque at 3 bar and maximum pressure. Operating temperature -20 - +80°C. Materials of Construction: Cap screws - 304 SS, Housing – Aluminum. End cap - Cast aluminum [3].</p>

**(b) Pressure measurement equipment**


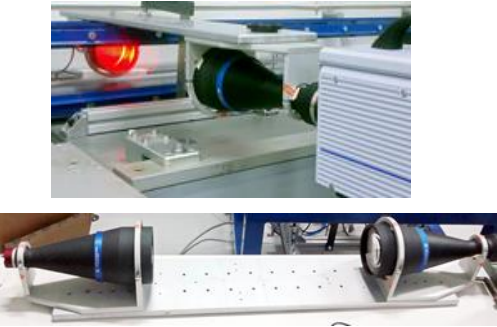
 	<p>Kulite: The XTM-190 miniature pressure transducer utilizes a metal diaphragm as a force collector with a Piezoresistive Sensor as its sensing element. With the threaded body, hexagonal head and O-ring seal, the XTM-190 is easy to mount and simple to apply. The small size and flush diaphragm permit direct installation of the transducer in the wall of pressure containers, tubes, pipes, etc., eliminating the need for costly, space-consuming hardware. The reference pressure source should be dry, noncorrosive gas [4].</p>
  	<p>Kistler quartz pressure sensor for measuring dynamic and quasistatic pressures up to 250 bars at temperatures up to 350 °C. The measured pressure acts through the diaphragm on the quartz crystal measuring element, which transforms the pressure <math>p</math> (bar) into an electrostatic charge <math>Q</math> (PC = picocoulomb). The stainless-steel diaphragm is welded flush and hermetically to the stainless-steel sensor body. The quartz elements are mounted in a highly sensitive arrangement (transversal effect) in the quartz chamber, which is welded hermetically to the body. The connector is tight and has a ceramic insulator. Kistler single-channel multi-range laboratory charge amplifier converts the electrical charge produced by piezoelectric sensors into a proportional voltage signal. This amplifier serves mainly to measure mechanical quantities, e.g. pressure, force or acceleration. The instrument can be supplied in a desktop or rackmount case [5].</p>

**(c) Triggering equipment**

	<p>Quantum composer plus Digital Delay-Pulse Generator with 8 independent outputs is designed to provide cutting edge, yet cost-effective solutions to generate and synchronize multiple pulses for a variety of applications. The delay and pulse width for each channel is independent and digitally controlled which makes the instrument ideal for situations that require synchronizing a number of different events. Flexible operating modes allow complete control of pulse outputs. More advanced features such as multiplexing allow the timing of all or several channels to be combined for complex pulse patterns [6].</p>
---	---



**(d) Image recording equipment**

	<p>The FASTCAM SA1.1 utilizes the same CMOS sensor with a 20µm pixel delivering an ISO light sensitivity 10,000 (monochrome) and 4,000 (color), both measured to the published ISO 12232 Ssat standard. Maintaining a square aspect ratio of 1024 x 1024 pixels for frame rates up to 5,400fps is extremely useful when observing events such as combustion through optical access windows [7]</p>
	<p>OPTO ENGINEERING, Telecentric TC lenses are specifically designed for accurate measurement and inspection of parts in a wide variety of industries. The system involves bi-telecentric optics and LTCLHP high-performance illuminator. The lenses were fixed to a slab with clamps. Using backlight illuminators with bi-telecentric lenses ensures incredibly sharp profiles and well-contrasted images, unlike common backlights [8]</p>

**(e) Concentration measurement equipment**

	<p>The XEN-5320 is an intelligent gas sensor for the measurement of gas composition, such as helium or hydrogen in air. The sensor is based on the measurement of the thermal conductivity of the ambient gas, using the proven thermal conductivity sensor XEN-TCG3880. To compensate for the influence of temperature and humidity, these are measured separately, and a correction is made for them in the micro-controller. Each device is factory calibrated (zeroed), the customer can re-zero. Gain adjustment is also possible. Standard the read-out and powering is done by wireless read-out (WIFI), with Li-ion battery power [9].</p>
---	--

## References

- [1] T. A. G. o. companies. ( 2009). *Variable Area Flowmeters: Purgemaster - Series 10A6100*. Available: [https://library.e.abb.com/public/d62cf6a3e7b311bac1257a92005c123a/D-FV-10A6100\\_5\(US\).pdf](https://library.e.abb.com/public/d62cf6a3e7b311bac1257a92005c123a/D-FV-10A6100_5(US).pdf)
- [2] Ritter. *DRUM-TYPE GAS METERS TG 1 STAINLESS STEEL • DATA-SHEET*. Available: <https://www.ritter.de/download/tg-1-stainless-steel.pdf/>
- [3] S. Company. ( 2017 ). *Swagelok Ball Valve Actuation* Available: <https://www.swagelok.com/downloads/webcatalogs/EN/MS-02-343.PDF>
- [4] Kulite. *Kulite Miniature Ruggedized Pressure Transducer* Available: <https://www.kulite.com/assets/media/2018/01/XTM-190.pdf>
- [5] K. I. AG. *Kistler Model 7001 Polystable Quartz High Temperature Pressure Sensor*. Available: [https://www.process-controls.com/intertechnology/Kistler/pdfs/Pressure\\_Model\\_7001.pdf](https://www.process-controls.com/intertechnology/Kistler/pdfs/Pressure_Model_7001.pdf)
- [6] Q. Composers. *Quantum Composers :9510+ Series Digital Delay Pulse Generators*. Available: [https://www.photonicsolutions.co.uk/upfiles/QC\\_9510.pdf](https://www.photonicsolutions.co.uk/upfiles/QC_9510.pdf)
- [7] Photron. *Photron high-speed cameras: FASTCAM SA1.1*. Available: <https://photron.com/fastcam-sa1-1/>
- [8] O. Engineering. (2015). *Telecentric TC lenses*. Available: <https://www.opto-e.com/products/matrix-detector-telecentric-lenses#Downloads>
- [9] X. Integration. (2018). *XEN-5320 TCG Sensor with can / usb / wifi read-out* Available: <http://www.xensor.nl/pdf/files/sheets/xen-5320-tcg-sensor.pdf>

## Appendix H

### EXPERIMENTAL STUDY OF LIGHT GAS DISPERSION IN A CHANNEL

Ibrahim, O.K.I., Vaagsaether, K. and Bjerketvedt, D.  
Department of Process, Energy and Environmental Technology,  
University of South-Eastern Norway,  
Kjølnes ring 56, Porsgrunn, 3918, Norway

Paper #216, 2019-04-04, First submission ICHS 2019 (<https://hvsafe.info/ichs2019/>)

#### ABSTRACT

Usage of hydrogen as fuel gives rise to possible accidental risks due to leakage and dispersion. The highest risk from hydrogen leak is the formation of a large volume of the hydrogen-air mixture, which could be ignited and leading up to a severe explosion. Prevention and control of formation and ignition of combustible hydrogen cloud necessitate sufficient knowledge of mechanisms of the hydrogen leak, dispersion, and over-pressures generated during ignition and explosion. This paper aims to investigate the momentum-controlled jet, the buoyancy-controlled wave and the parameters influence hydrogen concentration distribution in confined spaces. It demonstrates experimental results and analysis from helium and hydrogen dispersion in a channel. A set of experiments were carried out for the release of helium and hydrogen jets in a 3 m long channel to record their concentrations in the cloud by concentration sensors at different horizontal and vertical positions. Flow visualization technique was applied using shadowgraph to image the mixing process next to the release point and the helium-, hydrogen-air cloud shape at the middle of the channel. Moreover, results were used for comparison of helium and hydrogen concentration gradients. Experiments results show that swift mixing occurs at higher flow rates, smaller nozzle sizes, and downward release direction. Higher concentration recorded in the channel with negative inclination. Results also confirmed that hydrogen/ helium behavior pattern in the channel accords with mutual intrusion theory about gravity currents.

#### 1.0 INTRODUCTION

In recent years, there has been an increasing interest in hydrogen as a sustainable energy carrier because of growing concerns about fossil fuel dependence. Risks of fire and explosions are central safety considerations connected to the hydrogen application in the transport sector. The hazard of hydrogen explosion is a concern when it leaks in confined spaces such as garages and tunnels. Leak and dispersion of hydrogen in such spaces may result in origination and development of a risky hydrogen-air combustible cloud. For better development of risk mitigation requirements, it is essential to understand the processes involved during the hydrogen leak, dispersion, and explosion. Determination of the positions where the cloud could be ignited and the extent to which flame can accelerate depends on the concentration of hydrogen in the combustible cloud [1]. This study was designed to examine the hydrogen concentration distribution in a laboratory scale channel. Data for this study were collected using concentration sensors at six horizontal positions along the channel and five vertical locations on the channel side.

There is a potential risk for an unintended explosion when using hydrogen in dispersion tests. Therefore, Helium was selected for a major part of this study due to safety concerns. Helium is considered to resemble hydrogen since it has similar low density and high buoyancy (helium is twice dense as hydrogen, and they have about 8% difference in buoyancies). Helium and hydrogen volumetric flow rates were assumed to be equal in the prediction of hydrogen dispersion and explosion using helium. However, several studies were mentioned the difference between helium and hydrogen flow rates

between helium and hydrogen flow rates [2-5]. To use helium as a substitute for hydrogen, Jiaqing He et al. [2] suggested that differences in air-helium and air-hydrogen densities should be considered.

### 1.1 Momentum- and buoyancy-controlled jets

The hydrogen gas released in a channel will disperse by diffusive and buoyant forces. The influence of buoyancy on the gas wave is more significant than diffusivity at low-momentum hydrogen releases[6]. Therefore, highly concentrated with hydrogen and less dense gas cloud arises close to release point, and the variation in densities promotes buoyancy forces which cause the cloud to upsurge vertically and proceeds at the upper part of the channel. The hydrogen-rich cloud loses its inertia gradually and becomes buoyancy-driven. The mixing process with air either in the formation of the cloud or when the cloud propagates downstream occurs in nonhomogeneous mode. Thus, concentration decays along the jet axis and horizontally away from the release site[7].

### 1.2 Gravity currents and Froude scaling

Gravity currents generated in the horizontal flows due to density differences in the fluid under a gravitational field. An important kind of gravity current is the flow of less dense gas caused by the accidental release in tunnels or other semi-confined spaces. Density variations in a gravitational field generate buoyancy forces which cause the flow into horizontal motion and produce horizontal pressure gradients. The front zone formed by a gravity current is characterized by the presence of a relatively sharp line dividing the two fluids. The front shape of the cloud formed by a gravity current is influenced by the reverse ambient flow [8]. Turbulent mixing typically occurs at gravity current front, and the mixing process continues at the interface between the two fluids as the cloud spreads. According to J. E. Simpson analysis [8], three regions are observed at the front of gravity current, the upper layer where the less dense cloud is moving, bottom layer with air and the mixing region between these two layers. Fig.1 represents the shape of the pre-mixed cloud as it propagates after the gas injection into the channel.

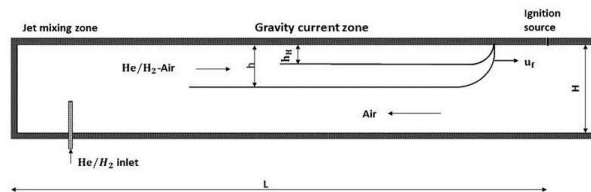


Figure 1. Schematic illustration of hydrogen/helium -air cloud formed by gravity current in the channel

Scaling techniques are extensively applied in researches of tunnel fire safety, and the major preserved dimensionless group in these researches is the Froude number. The dimensionless Froude number is the ratio between inertia and gravity forces exerting influence on the fluid flow, and it can be used to describe the dispersion of hydrogen/helium in a channel [9]. Froude number is related to the front velocity of a gravity current as

$$Fr = \frac{u}{\sqrt{gl}}, \tag{1}$$

where  $u$  is the front velocity,  $g$  is the acceleration due to gravity, and  $l$  is a characteristic length scale.

The front velocity of the cloud in the channel is  $u_f$ , and the characteristic length scale,  $l$ , can be represented as the theoretical layer of 100% hydrogen/helium,  $h_H$ . The reasoning for this option is that the front velocity is not affected by the mutual intrusion in dispersion process since the increase in the height of the cloud depends on the hydrogen/ helium flow rate and balanced by the decrease in cloud density [10, 11]. The gas flow rate into the channel,  $Q$  [ $m^3/s$ ] can be connected to the unmixed layer,  $h_H$ , as



$$Q = u_f \cdot h_H \cdot w, \quad (2)$$

where  $w$  is the width of the channel. Substitution of the unmixed layer,  $h_H$ , in the Froude number expression, gives

$$Fr = \sqrt{u_f^3 \cdot w/gQ}, \quad (3)$$

The average cloud front velocity,  $u_f$ , can be expressed in terms of the distance covered by the cloud from the release point to reach the sensor's position (or ignition point),  $L$  [m], and the time required to reach this point,  $\Delta t$  [s]. thus, Froude number can be rewritten as

$$Fr = \sqrt{\left(\frac{L}{\Delta t}\right)^3 \cdot w/gQ}, \quad (4)$$

## 2.0 EXPERIMENTAL SETUP

### 2.1 Channel description

Experiments executed in a horizontal rectangular cuboid channel with dimensions: 3 m length, 0.1 m width, and height. The channel was made of coated steel with transparent polycarbonate sidewalls. It was open on one side and closed in the other. The volume of the channel was 0.03 m<sup>3</sup>. Fig.2 represents a schematic design of the channel, indicating the positions of concentration measurement sensors, and Fig.3 shows an oblique image of its laboratory setup.

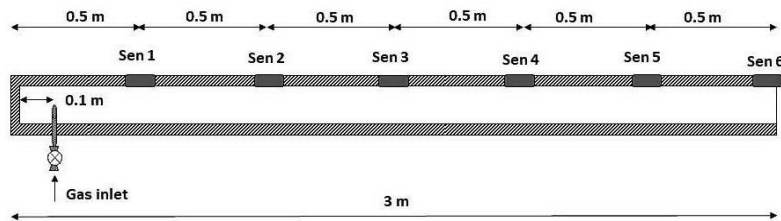


Figure 2. Schematic design of the channel with sensors positions



Figure 3. An oblique image of the channel setup

### 2.2 Helium injection

Helium was provided from helium standard 180 bar cylinder. The gas flow was adjusted by Purgemaster volume flow meter with releasing flow rate in the range of 5 to 90 Ndm<sup>3</sup>/ min. The flow meter was calibrated before measurements start by Ritter drum-type TG 10/1. Then the gas was injected into the channel upwards or downwards through a 4 mm pipe, which located at centerline 100 mm from the closed end and had 50 mm height in the channel. At the exit of the 4 mm pipe, different circular nozzles with diameters 2.5, 1.0, and 0.5 mm were used for injection of helium into the channel.

### 2.3 Measurement devices

Measurement of helium concentration as volume percentage was recorded by XEN-5320 gas sensor for determining of gas composition Fig.4 (left) The XEN-5320 is an integrated sensor based on the measurement of the thermal conductivity of the gas. It automatically corrects for the temperature and humidity. The sensor was WIFI read out, connected to a laboratory WIFI network and it sent the measurements to a specific computer program (Xen-5320 LabView Standard v3.20 WIFI). Sensors were located at six different positions along the channel. The first one was located 0.4 m from the release point, and the others were positioned 0.5 m from each other (Fig.4 (right)).

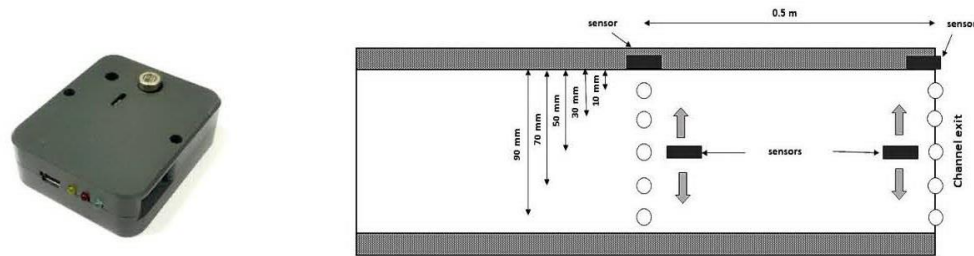


Figure 4. Concentration sensor XEN-5320 from Xensor Integration, (left) and Sensors positions for measuring He concentration at the different vertical location at 500 mm from the channel exit and at the exit, (right).

Helium volume fractions were similarly recorded at five vertical positions, at 10, 30, 50, 70 and 90 mm from the ceiling, at the horizontal location, 2.5 and 3 m from the closed channel end. Figure VV lustrates the vertical sensor's positions at two horizontal sites

### 2.4 Flow visualization technique

Flow imaging systems provide a technique to visualize changes in refractive index depending on the density variation of transparent media [12]. The shadowgraph lens system (SLS) was used in this study in which a shadow projected from refractive deflection of a light ray creates a bright position on the recording plane while undeflected rays remain dark. Consequently, a visible pattern of lighting variations is generated on the recorded plane. Fig. 5 shows are drawing a representation of shadowgraph arrangement, on the left-hand side.

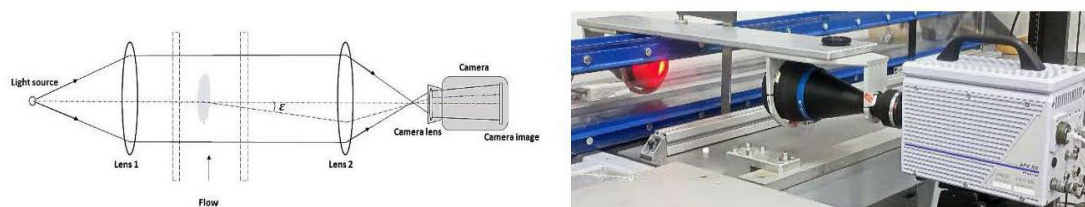


Figure 5. Conceptual drawing of Background-Oriented Schlieren (BOS), (left) and the configuration of the shadowgraph system used in the experiments, (right)

Shadowgraph system was utilized to visualize the air-helium cloud formation next to the release point and the shape of the cloud, once it propagated passing the lenses location at 1.5 m from the channel, closed end. The system includes lenses from OPTO ENGINEERING, Telecentric TC lenses, and LTCLHP high-performance illuminator to illuminate objects imaged by Telecentric lenses. The lenses were fixed to a slab with clamps. High-speed digital video camera, FastCam APX RS, was linked to the lenses for image recording. Fig. 5, on the right side, present the image of the system fixed at the middle of the channel. 1.5 m from the channel closed end.

between helium and hydrogen flow rates [2-5]. To use helium as a substitute for hydrogen, Jiaqing He et al. [2] suggested that differences in air-helium and air-hydrogen densities should be considered.

### 1.1 Momentum- and buoyancy-controlled jets

The hydrogen gas released in a channel will disperse by diffusive and buoyant forces. The influence of buoyancy on the gas wave is more significant than diffusivity at low-momentum hydrogen releases[6]. Therefore, highly concentrated with hydrogen and less dense gas cloud arises close to release point, and the variation in densities promotes buoyancy forces which cause the cloud to upsurge vertically and proceeds at the upper part of the channel. The hydrogen-rich cloud loses its inertia gradually and becomes buoyancy-driven. The mixing process with air either in the formation of the cloud or when the cloud propagates downstream occurs in nonhomogeneous mode. Thus, concentration decays along the jet axis and horizontally away from the release site[7].

### 1.2 Gravity currents and Froude scaling

Gravity currents generated in the horizontal flows due to density differences in the fluid under a gravitational field. An important kind of gravity current is the flow of less dense gas caused by the accidental release in tunnels or other semi-confined spaces. Density variations in a gravitational field generate buoyancy forces which cause the flow into horizontal motion and produce horizontal pressure gradients. The front zone formed by a gravity current is characterized by the presence of a relatively sharp line dividing the two fluids. The front shape of the cloud formed by a gravity current is influenced by the reverse ambient flow [8]. Turbulent mixing typically occurs at gravity current front, and the mixing process continues at the interface between the two fluids as the cloud spreads. According to J. E. Simpson analysis [8], three regions are observed at the front of gravity current, the upper layer where the less dense cloud is moving, bottom layer with air and the mixing region between these two layers. Fig.1 represents the shape of the pre-mixed cloud as it propagates after the gas injection into the channel.

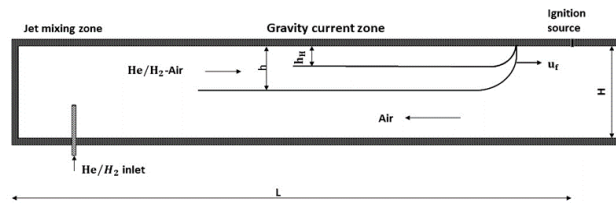


Figure 1. Schematic illustration of hydrogen/helium -air cloud formed by gravity current in the channel

Scaling techniques are extensively applied in researches of tunnel fire safety, and the major preserved dimensionless group in these researches is the Froude number. The dimensionless Froude number is the ratio between inertia and gravity forces exerting influence on the fluid flow, and it can be used to describe the dispersion of hydrogen/helium in a channel [9]. Froude number is related to the front velocity of a gravity current as

$$Fr = \frac{u}{\sqrt{gl}}, \quad (1)$$

where  $u$  is the front velocity,  $g$  is the acceleration due to gravity, and  $l$  is a characteristic length scale.

The front velocity of the cloud in the channel is  $u_f$ , and the characteristic length scale,  $l$ , can be represented as the theoretical layer of 100% hydrogen/helium,  $h_H$ . The reasoning for this option is that the front velocity is not affected by the mutual intrusion in dispersion process since the increase in the height of the cloud depends on the hydrogen/ helium flow rate and balanced by the decrease in cloud density [10, 11]. The gas flow rate into the channel,  $Q$  [ $m^3/s$ ] can be connected to the unmixed layer,  $h_H$ , as



$$Q = u_f \cdot h_H \cdot w, \quad (2)$$

where  $w$  is the width of the channel. Substitution of the unmixed layer,  $h_H$ , in the Froude number expression, gives

$$Fr = \sqrt{u_f^3 \cdot w/gQ}, \quad (3)$$

The average cloud front velocity,  $u_f$ , can be expressed in terms of the distance covered by the cloud from the release point to reach the sensor's position (or ignition point),  $L$  [m], and the time required to reach this point,  $\Delta t$  [s]. thus, Froude number can be rewritten as

$$Fr = \sqrt{\left(\frac{L}{\Delta t}\right)^3 \cdot w/gQ}, \quad (4)$$

## 1.0 EXPERIMENTAL SETUP

### 2.1 Channel description

Experiments executed in a horizontal rectangular cuboid channel with dimensions: 3 m length, 0.1 m width, and height. The channel was made of coated steel with transparent polycarbonate sidewalls. It was open on one side and closed in the other. The volume of the channel was 0.03 m<sup>3</sup>. Fig.2 represents a schematic design of the channel, indicating the positions of concentration measurement sensors, and Fig.3 shows an oblique image of its laboratory setup.

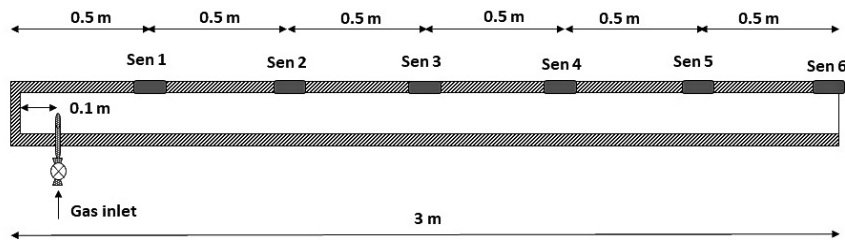


Figure 2. Schematic design of the channel with sensors positions



Figure 3. An oblique image of the channel setup

### 2.2 Helium injection

Helium was provided from helium standard 180 bar cylinder. The gas flow was adjusted by Purgemaster volume flow meter with releasing flow rate in the range of 5 to 90 Ndm<sup>3</sup>/ min. The flow meter was calibrated before measurements start by Ritter drum-type TG 10/1. Then the gas was injected into the channel upwards or downwards through a 4 mm pipe, which located at centerline 100 mm from the closed end and had 50 mm height in the channel. At the exit of the 4 mm pipe, different circular nozzles with diameters 2.5, 1.0, and 0.5 mm were used for injection of helium into the channel.



### 2.3 Measurement devices

Measurement of helium concentration as volume percentage was recorded by XEN-5320 gas sensor for determining of gas composition Fig.4 (left) The XEN-5320 is an integrated sensor based on the measurement of the thermal conductivity of the gas. It automatically corrects for the temperature and humidity. The sensor was WIFI read out, connected to a laboratory WIFI network and it sent the measurements to a specific computer program (Xen-5320 LabView Standard v3.20 WIFI). Sensors were located at six different positions along the channel. The first one was located 0.4 m from the release point, and the others were positioned 0.5 m from each other (Fig.4 (right)).

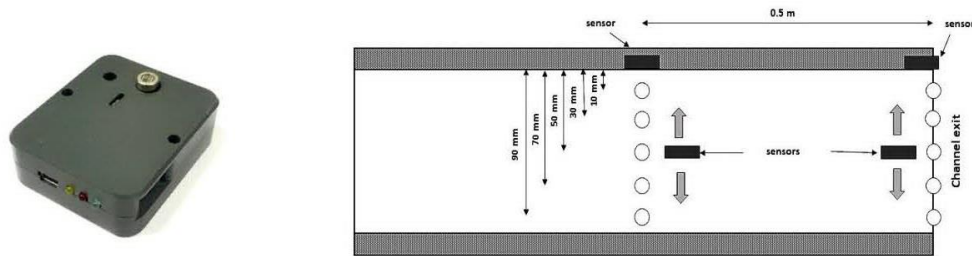


Figure 4. Concentration sensor XEN-5320 from Xensor Integration, (left) and Sensors positions for measuring He concentration at the different vertical location at 500 mm from the channel exit and at the exit, (right).

Helium volume fractions were similarly recorded at five vertical positions, at 10, 30, 50, 70 and 90 mm from the ceiling, at the horizontal location, 2.5 and 3 m from the closed channel end. Figure VV lustrates the vertical sensor's positions at two horizontal sites

### 2.4 Flow visualization technique

Flow imaging systems provide a technique to visualize changes in refractive index depending on the density variation of transparent media [12]. The shadowgraph lens system (SLS) was used in this study in which a shadow projected from refractive deflection of a light ray creates a bright position on the recording plane while undeflected rays remain dark. Consequently, a visible pattern of lighting variations is generated on the recorded plane. Fig. 5 shows are drawing a representation of shadowgraph arrangement, on the left-hand side.

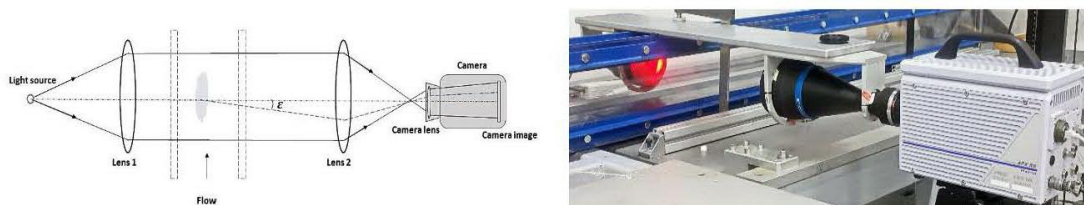


Figure 5. Conceptual drawing of Background-Oriented Schlieren (BOS), (left) and the configuration of the shadowgraph system used in the experiments, (right)

Shadowgraph system was utilized to visualize the air-helium cloud formation next to the release point and the shape of the cloud, once it propagated passing the lenses location at 1.5 m from the channel, closed end. The system includes lenses from OPTO ENGINEERING, Telecentric TC lenses, and LTCLHP high-performance illuminator to illuminate objects imaged by Telecentric lenses. The lenses were fixed to a slab with clamps. High-speed digital video camera, FastCam APX RS, was linked to the lenses for image recording. Fig. 5, on the right side, present the image of the system fixed at the middle of the channel. 1.5 m from the channel closed end.

### 2.5 Experimental models

Various sets of experiments were performed to investigate the influence of different parameters on the helium concentration distribution in the channel. Parameters included flow rate, nozzle size, vertical concentration distribution, injection direction, and channel inclination. All parameters in the process are interrelated. Therefore, concentration measurements were divided into four models, helium horizontal, helium vertical, helium dispersal in inclined channel and helium/hydrogen horizontal concentration distribution. Horizontal measurements involved recording the concentration by sensors at six locations along the channel, as it defines in Fig. 2, for different flow rates, nozzle sizes and release directions: upward, U, and downwards, D. Table 1 gives an overview of the horizontal measurement's matrix.

Table 1. The first model experimental matrix.

Flow rate, dm <sup>3</sup> /min	Nozzle size							
	0.5 mm		1 mm		2.5 mm		4 mm pipe	
5	U	D			U	D	U	
15	U	D			U	D	U	
40	U	D	U	D	U	D	U	D

The second model is vertical concentration measurements at two horizontal locations on the channel side, 2.5 m from the channel closed end and at the exit. Sensor's vertical positions were 0, 10, 30, 50, 70 and 90 mm from the ceiling as presented in Fig. 4 (right). Table 2 defines the parameters used during the measurements.

Table 2. experimental model for vertical concentration distribution.

Parameters	Nozzle size	
	1 mm	Pipe 4 mm
Flow rate, dm <sup>3</sup> /min	5, 15 and 40	40
Release direction	D	U and D
Position from the channel end, m	2.5 and 3	2.5 and 3

The third model is the determination of helium concentration along the inclined channel. Measurements were done for the channel with an inclination of 10 and -10 degrees. Fig.6 illustrates a drawing of the inclined channel towards the exit ( $\varphi = -10^\circ$ ). Helium released downward at flow rates 15 and 40 Ndm<sup>3</sup>/min through a pipe diameter 4 mm.

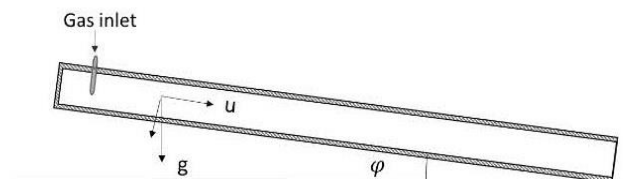


Figure 6. schematic representation of the channel with an inclination of  $-10^\circ$

The fourth model covered the measurements of helium and hydrogen concentrations as it explained in the horizontal helium model with the same parameters in Table 1. In this model, pneumatic valve, Swagelok, connected to the inlet pipe for better control of gas flow rate. The pneumatic valve was triggered together with a pressure sensor to record the pressure at the valve during the gas release.

### 3.0 RESULT AND DISCUSSION

#### 3.1 Flow rate effect

Results from the sensor's measurements for helium concentration along the channel at flow rates 5, 15 and 40 Ndm<sup>3</sup>/min and 3 minutes release time are shown in Fig. 7. The figure shows an apparent increase in helium concentration recorded by sensors at all measurements locations with an increase in flow rate. Simultaneously, the time between the sensor's recording starts decreases. This indicates a rise in the cloud's velocity with an increase in flow rates.

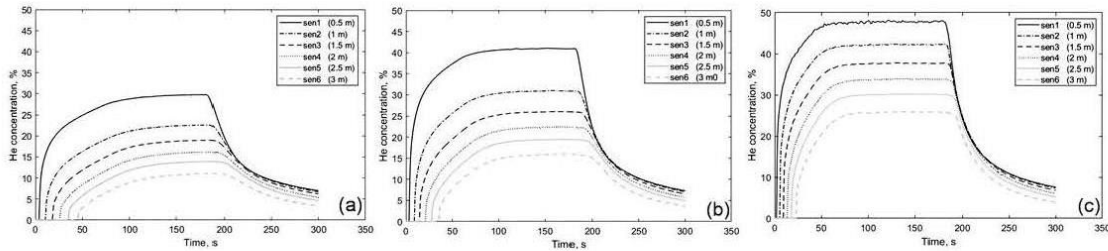


Figure 7. Helium output concentration over time for upward release through 4 mm diameter pipe and at flow rates: (a) 5, (b) 15 and (c) 40 Ndm<sup>3</sup>/min

Concentration decay lengthways the channel signifies that helium-air cloud loses its inertia while it propagates through the channel and turns to be buoyancy-driven. This process decays with an increase in the flow rate as can be seen from (a) to (c) graphs in Fig. 7.

The concentration distribution of helium vertically in the channel was determined by recording the concentration in two horizontal positions, at 2.5 m from the channel closed end and the channel exit. Vertical positions were 0,10, 30, 50, 70, 90 mm from the ceiling. Fig.8 shows helium output concentration as the function of time at cited vertical locations for downward release through 2.5 mm nozzle and at 2.5 m from the closed end.

Figure 8. Distribution of helium concentration vertically over time for downward release through 2.5 mm nozzle size and at flow rates: (a) 5, (b) 15 and (c) 40 Ndm<sup>3</sup>/min

Over-all constructed concentration profiles with different flow rates were observed unchanged. Helium concentration moved upward close to the ceiling from 13.8 % in (a) to 28.2 % in (c) while the flow rate was raised from 5 in (a) to 40 dm<sup>3</sup>/min in (c) graphs in Fig. 8. This indicates that concentration decays horizontally and vertically while the cloud is propagating in the channel.

#### 3.2 Nozzle size effect

Sensors measurements for helium dispersal in the channel were done using different nozzle sizes, 0.5, 1, 2.5 mm and pipe diameter 4mm. Fig.8 illustrates helium concentration over 5 minutes for downward release at 40 Ndm<sup>3</sup>/min for four defined nozzle sizes. As evident from the graphs in Fig. 9, the upper lines are becoming more undulate, and the differences between two upper concentration lines decrease from 1.86% in the graph (d) to 1.15% in the graph (a), with a decrease in nozzle size, from 4 to 0.5 mm. This specifies more rapid mixing of helium with air close to the release point as the nozzle size

decreases due to the rise in flow velocity. It can also be observed from the time that lines are level out, 87 s in the graph (a) to 71 s, in (d).

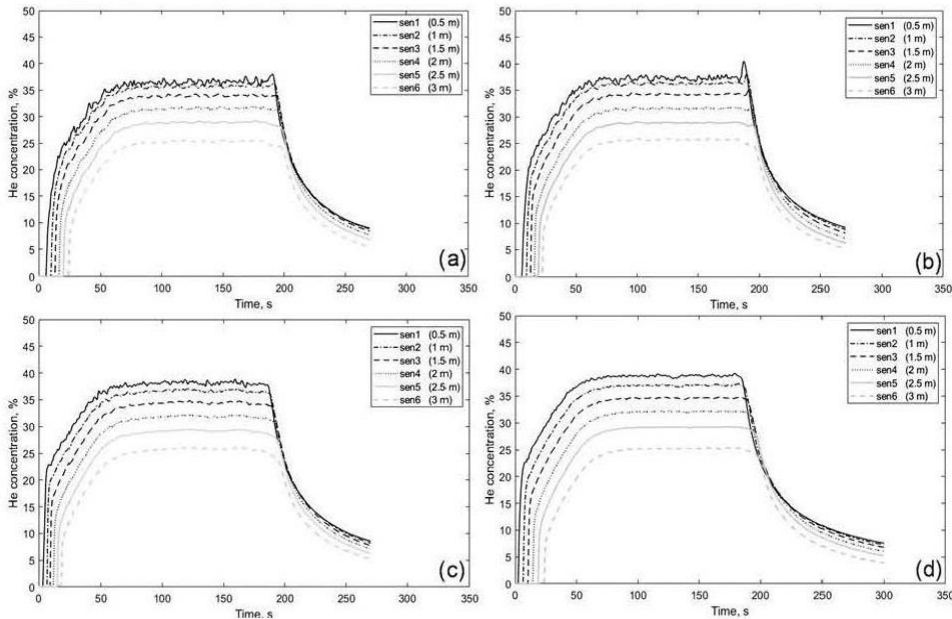


Figure 9. Output concentration over time of downward helium release at 40 Ndm<sup>3</sup>/min and through nozzle sizes: (a) 0.5, (b) 1, (c) 2.5 mm and (d) pipe diameter 4 mm.

Fig.10 demonstrates helium concentration vertical measurements for 3 minutes downward release at a flow rate of 40 Ndm<sup>3</sup>/min through 2.5 mm nozzle size and 4 mm pipe. The trends presented in this figure are like those in Fig. 7. The concentration slightly increased with nozzle size has been changed from 2.5 mm to 4 mm. Simultaneously, the difference between the two upper sensor's readings line increased. This may be explained by the concentration drop as the mixing process developed faster with a smaller nozzle size.

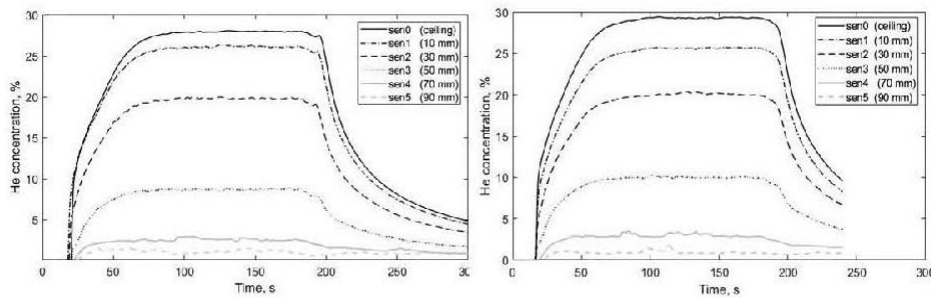


Figure 10. Vertical concentration distribution over time of downward helium release at 40 Ndm<sup>3</sup>/min and through nozzle sizes, 2.5 mm (left) and pipe diameter 4 mm (right).

### 3.3 The influence of release direction

Changes in helium concentration distribution were identified by helium upward and downward injections at different flow rates and nozzle sizes. Fig. 11 demonstrates helium concentration over time for releases through a 2.5 mm nozzle size at a flow rate of 15 Ndm<sup>3</sup>/min. it is apparent from the graphs presented in Fig. 11 that the concentration recorded by the first sensor is higher for upward release than for downward. This happened because of the mixing process is higher near the release point and mainly induced by momentum. Formed mixture by downward release changes direction upwards due to density difference and mixes additionally with air while it proceeds downstream at the upper part of the channel.



No differences in vertical distribution have been observed between upward and downward releases away from the release point.

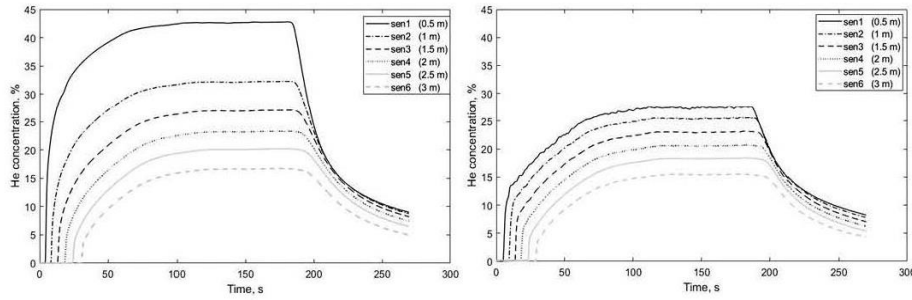


Figure 11. Output helium concentration versus time for upward release, left and downward, right at flow rate  $15 \text{ Ndm}^3/\text{min}$  and  $2.5 \text{ mm}$  nozzle size.

### 3.4 Channel inclination

The channel was inclined by  $10^\circ$  and  $-10^\circ$  in order to analyze how inclination affect concentration distribution in the channel. Helium was released downward through  $4 \text{ mm}$  pipe at  $15$  and  $40 \text{ Ndm}^3/\text{min}$ . Descriptive data were generated for all sensor's positions depicting dissimilarity of the two tilted channel structures. Fig. 12 displays helium concentration over time for downward releases in the inclined channel by  $10^\circ$  degrees, left and  $-10^\circ$  degrees, right at  $15 \text{ Ndm}^3/\text{min}$ .

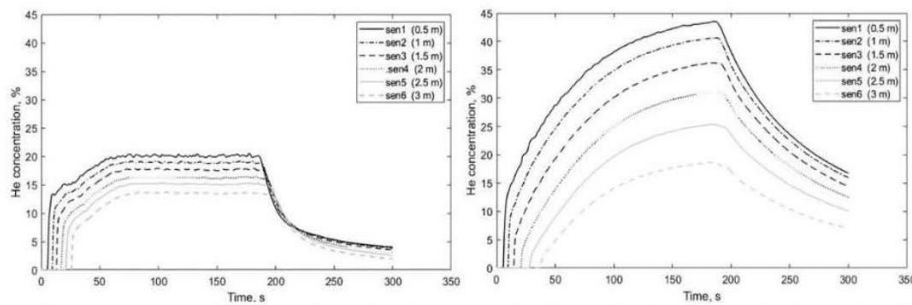


Figure 12. Helium concentration over time for downward release in the channel with an inclination of  $10^\circ$ , left and  $-10^\circ$ , right at  $15 \text{ Ndm}^3/\text{min}$  and through  $4 \text{ mm}$  pipe.

From the data in the above graphs, it is apparent that helium concentration is swiftly rising and reach much higher levels in an inclined channel by  $-10^\circ$  than by  $10^\circ$ . Furthermore, the concentration lines are situated closer to each other for the channel with positive inclination, left than with negative inclination, right. The observed differences in concentrations could be attributed to the rapid mixing process in the positive channel inclination. In the channel with negative inclination, the air inflows and mixes with helium is affected by gravity leading up to a reduction in the mixing intensity and growth of the cloud leading-front propagation rate. This outcome can be well observed comparing positive and negative channel inclination with horizontal channel position. Fig. 13 compare helium concentration distribution in an inclined channel by  $10^\circ$ , horizontal channel and inclined channel by  $-10^\circ$ .

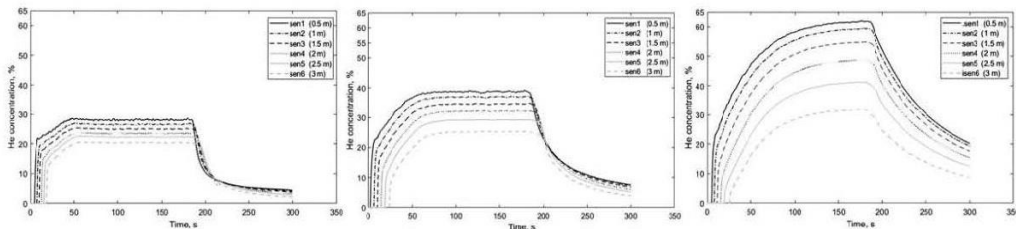


Figure 13. Helium concentration over time for downward release through  $4 \text{ mm}$  pipe at  $40 \text{ Ndm}^3/\text{min}$  and in the channel with an inclination of  $10^\circ$ , left, horizontal, middle and inclination of  $-10^\circ$ , right.

### 3.5 Mixing process

As expected, the results of the experiments show that helium mixes with air more rapidly at higher flow rates, smaller nozzle sizes, and downward release direction. Dispersion of helium in the channel characterized by the formation of inhomogeneous and stratified cloud. The mixing phenomena primarily start rapidly near the injection pipe and can be described as jet momentum- induced mixing. The cloud is developed around the injection pipe with high helium concentration and less dense than air. Subsequently, the cloud starts to rise due to buoyancy induced by density difference. Buoyancy-induced mixing continues as the cloud propagates through the channel creating a mixing zone as a line dividing the two fluids. In an attempt to visualize described phenomena, shadowgraph lens system was performed as defined in section (2.4) and the result is shown in Fig.14. Fig. 14 shows images of concentration gradients at the upper part of the channel after helium release at a flow rate of 50 dm<sup>3</sup>/min for 5.4 seconds.

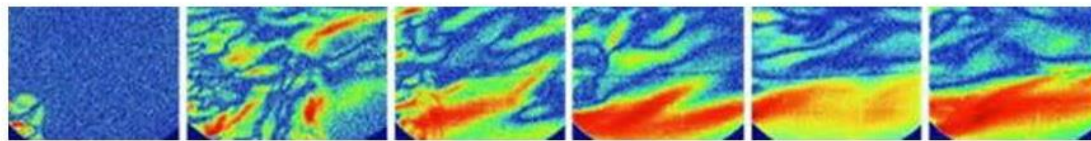


Figure 14. Helium concentration gradients next to the release point visualized by shadowgraph for downward release at 50 Ndm<sup>3</sup>/min through pipe diameter 4 mm.

Above images designate a complex mode of mixing flow pattern next to injection pipe and show the developing of mixing zone to form a layer divided the two fluids as specified in the gravity currents theory in section (1.3). Furthermore, they also express the inhomogeneous and stratified nature of the cloud in the channel.

### 3.6 Comparison of hydrogen and helium results

Measurements of hydrogen and helium concentration along the channel were performed for 3 minutes release time through pipe diameter 4 mm and flow rates, 5, 15 and 40 Ndm<sup>3</sup>/min. The results of these measurements are shown in Fig. 15 and Fig. 16. Hydrogen concentration is higher from (a) to (c) graphs in Fig. 15 compared with corresponding graphs for helium in Fig. 16. These results are likely to be related to the differences in density hydrogen/air and helium/air which has been reported by He et al. [2].

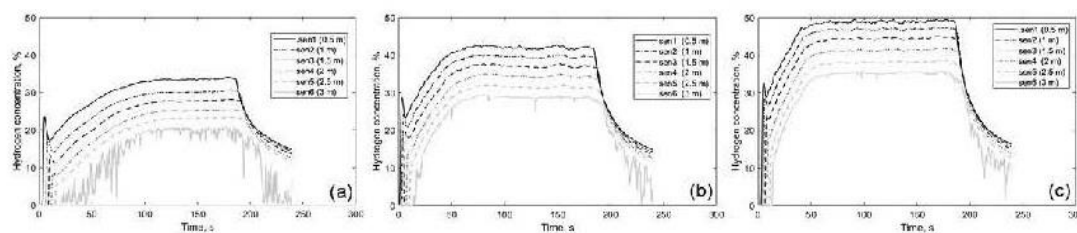


Figure 15. Hydrogen concentration over time for downward releases at flow rates, 5 (a), 15 (b) and 40 Ndm<sup>3</sup>/min (c), through pipe diameter 4 mm.

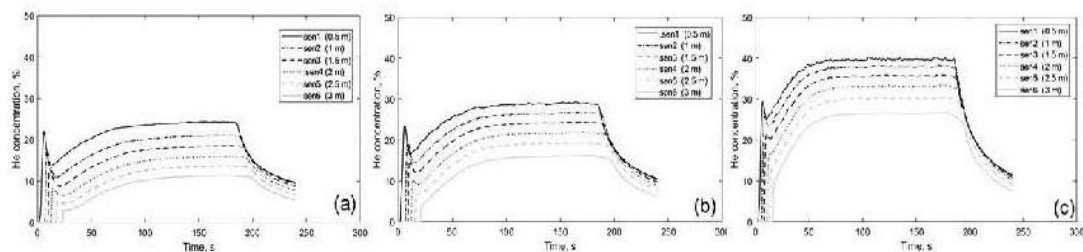


Figure 16. Helium concentration over time for downward releases through 4 mm pipe at flow rates, 5 (a), 15 (b) and 40 Ndm<sup>3</sup>/min (c).



Comparing hydrogen and helium releases at low flow rates is given in graphs (a) in Fig.15 and Fig.16. The hydrogen concentration is slightly higher than that for helium, but they behave differently at the channel exit. The lowest concentration line for hydrogen in Fig.15 is rippling, which denotes higher mixing of the hydrogen-air cloud with air at the channel exit than for helium-air cloud.

A comparison of the hydrogen-air cloud shape and front velocity and the helium-air cloud was drawn by implementing shadowgraph technique as described in section (2.4) at the middle of the channel, 1.5 m from the closed end, and the results are shown in Fig.17. Hydrogen and helium were released downward through 4 mm pipe at a flow rate of 40 Ndm<sup>3</sup>/min.

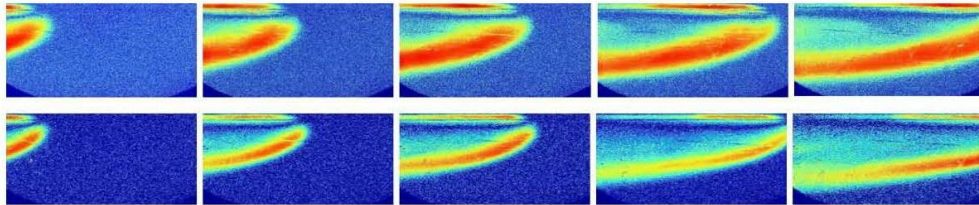


Figure 17. Concentration gradients of helium, upper series, and hydrogen, lower series, visualized by shadowgraph while the cloud propagating through the channel for at 1.5 m from the channel closed end for downward releases through 4 mm pipe and flow rate 40 Ndm<sup>3</sup>/min.

The most interesting aspect of these images is the thickness of the mixing zone, which represents the higher gradient in the images, is thicker for helium-air cloud than that for hydrogen. This is likely to be related to the difference in front velocity of the clouds which was found to be 0.198 m/s for helium-air cloud compared to 0.181 for the hydrogen-air cloud.

### 3.7 Froude scaling

Froude number is used to describe the pattern of the flows driven by buoyancy. Several studies have explored the relation of inertia forces to buoyancy by Froude number. For instance, Houf et al. [13] and Sommersel et al. [11, 14]. To verify whether the experimental results accord with previous researches findings, the Froude number was calculated using formula (4) for different hydrogen and helium flow rates. Time in the formula defined as the start time recorded by each sensor relative to the first one. Results from calculations are shown in Fig.18.

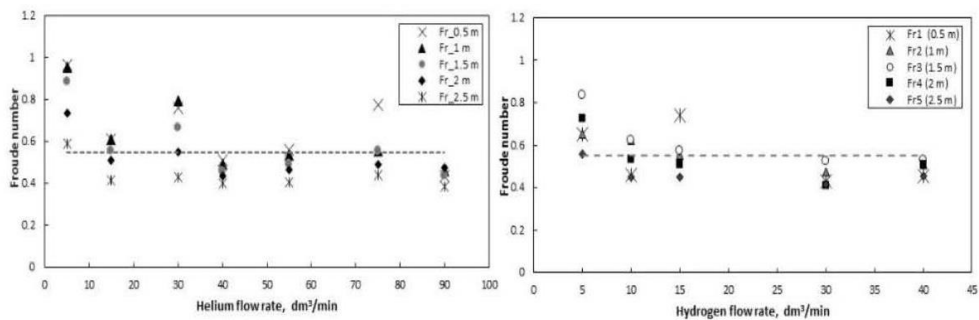


Figure 18. Froude numbers for downward releases of helium, (left) and hydrogen, (right) through pipe diameter 4 mm at a flow rate 40 Ndm<sup>3</sup>/min.

Calculated average Froude number was found to be 0.55 which corresponds dotted lines in Fig. 18. In order to assess how thoroughly the experimental time data accord with theoretical calculations of Froude number, the time was computed for the obtained average Froude number. Fig.19 compares the time calculated theoretically by applying the average Froude number, the solid lines, with experimentally recorded data for helium releases, left and hydrogen, right.

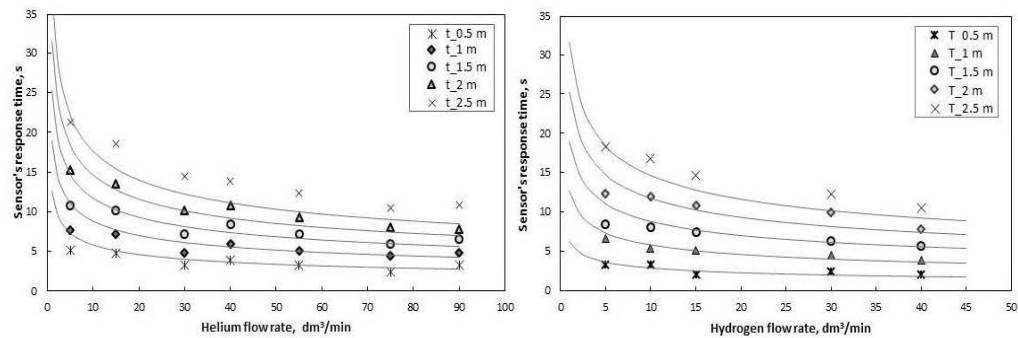


Figure 19. Sensor's response time versus flow rate for helium releases (left) and hydrogen (right). Solid lines represent calculated time values for  $Fr = 0.55$ .

There is a difference between obtained Froude number for hydrogen experiments and the previous results reported by Sommersel et al. [11, 14] in which the time determined at the time of ignition from fast camera recording videos and the Froude number has been quantified to be 0.68. A possible explanation for this difference in results might be the time taken by the sensors to measure and record the reading and that for electrode spark and video recording. These results of Froude number so far have only been found from concentration measurements and need to be compared with additional results from ignition experiments under the same conditions which are already underway.

#### 4 CONCLUSION

The present study is designed to investigate the concentration distribution of dispersed hydrogen in partly confined spaces and the parameters influence the concentration in the hydrogen-air cloud.

A sequence of experiments was carried out on laboratory scale three-meter-long steel channel with transparent polycarbonate sidewalls. A quantitative approach was employed for assessment of helium and hydrogen concentration distribution along the channel by using WIFI read out concentration sensors. Concentrations were measured at various horizontal and vertical injection positions for releases at different flow rates, through different nozzle sizes and different injection directions. Flow visualization technique was applied with the assistance of shadowgraph in this study to record an image of the concentration gradients of the mixing process next to the release point and the cloud propagation at the middle of the channel.

The results of this study indicate that the mixing of helium and hydrogen with air occur rapidly at higher flow rates, smaller nozzle sizes, and downward release direction. Moreover, these experiments confirmed that jet momentum- induced mixing happen close to release point and wave buoyancy-induced, away from it. Dispersion of helium in the channel characterized by the formation of inhomogeneous and stratified cloud. The relevance of mutual intrusion theory for gravity currents is clearly supported by flow imaging results.

The result of the Froude number is not in complete accord with results from previous studies and further investigations by different methods in progress to re-evaluate the findings.

Overall, this study contributes to the existing knowledge of hydrogen dispersion in confined spaces by providing practical data for further analyses.



## REFERENCES

- [1] L. Cadwallader and J. Herring, *Safety Issues with Hydrogen as a Vehicle Fuel*. Lockheed Martin Idaho Technologies Company, 1999.
- [2] J. He, E. Kokgil, L. Wang, and H. D. Ng, "Assessment of similarity relations using helium for prediction of hydrogen dispersion and safety in an enclosure," *International Journal of Hydrogen Energy*, vol. 41, no. 34, pp. 15388-15398, 2016/09/14/ 2016.
- [3] W. M. Pitts, J. C. Yang, and M. G. Fernandez, "Helium dispersion following release in a 1/4-scale two-car residential garage," *International Journal of Hydrogen Energy*, vol. 37, no. 6, pp. 5286-5298, 2012/03/01/ 2012.
- [4] M. R. Swain and J. Shriber, *Comparison of Hydrogen, Natural Gas, Liquefied Petroleum Gas, and Gasoline Leakage in a Residential Garage*. 1998.
- [5] G. Bernard-Michel and D. Houssin-Agbomson, "Comparison of helium and hydrogen releases in 1 m<sup>3</sup> and 2 m<sup>3</sup> two vents enclosures: Concentration measurements at different flow rates and for two diameters of injection nozzle," *International Journal of Hydrogen Energy*, vol. 42, 2016.
- [6] V. Molkov, *Fundamentals of Hydrogen Safety Engineering*. HySafer center -university of Ulster, 2012.
- [7] HySafe. (2009). *Accidental Phenomena and Consequences -Section 1.01-Release of Hydrogen*. Available: [https://www.hysafe.org/download/1003/BRHS\\_Chap3\\_release\\_version%2009\\_0.pdf](https://www.hysafe.org/download/1003/BRHS_Chap3_release_version%2009_0.pdf)
- [8] J. E. Simpson, *Gravity Currents: In the Environment and the Laboratory*. Cambridge University Press, 1999.
- [9] H. Ingason, Y. Li, and A. Lönnemark, *Tunnel Fire Dynamics*. New York: Springer science media New York, 2015.
- [10] T. K. Fannelöp, *Fluid Mechanics for Industrial Safety and Environmental Protection (Industrial Safety Series)*. Elsevier Science, 1994.
- [11] B. D. Sommersel O.K, Vaagsaether K., Fannelop T.K., "Experiments with release and ignition of hydrogen gas in a 3 m long channel," *International Journal of Hydrogen Energy*, vol. 34, no. 14, pp. 5869-74, 2009.
- [12] A. Mazumdar, "Principles and Techniques of the Schlieren Systems.," Columbia University New York, 2013.
- [13] W. G. Houf and R. Schefer, *Analytical and experimental investigation of small-scale unintended releases of hydrogen*. 2008, pp. 1435-1444.
- [14] O. K. Sommersel, *Hydrogen leaks in partially confined spaces - dispersion and explosions*. Porsgrunn: University College of Southeast Norway, 2017.